

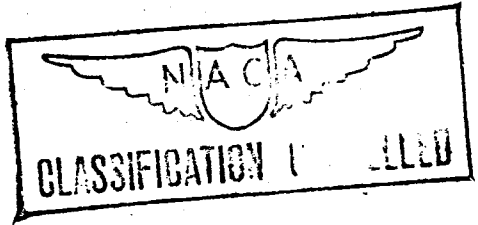
*Library*  
MR No. L5029b

1810.5  
PY-2/2

5 1945

NATIONAL ADVISORY COMMITTEE FOR AERONAUTICS

~~RESTRICTED~~



Restricted Abolished per  
E.O. 10501 dated Dec. 15, 1953

MEMORANDUM REPORT

for the

Bureau of Aeronautics, Navy Department

WIND-TUNNEL TESTS OF A PORTION OF A PV-2

HELICOPTER ROTOR BLADE

By W. B. Kemp

Langley Memorial Aeronautical Laboratory  
Langley Field, Va.

~~CLASSIFIED DOCUMENT~~

~~This document contains classified information affecting the National Defense of the United States within the meaning of the Espionage Act, Title 18, U.S.C. and 50. Its transmission or the revelation of its contents in any manner to an unauthorized person is prohibited by law. This document and its contents are imparted only to personnel in the military services of the United States, appropriate civilian officers and employees of the Federal Government who have a legitimate interest therein, and to United States citizens of known loyalty and discretion who, in necessity, must be informed thereof.~~

X  
X  
X



APR 5 1945

NACA LIBRARY  
LANGLEY MEMORIAL AERONAUTICAL LABORATORY

~~RESTRICTED~~

## NATIONAL ADVISORY COMMITTEE FOR AERONAUTICS

MEMORANDUM REPORT

for the

Bureau of Aeronautics, Navy Department

WIND-TUNNEL TESTS OF A PORTION OF A PV-2

HELICOPTER ROTOR BLADE

By W. B. Kemp

## SUMMARY

A portion of a PV-2 helicopter rotor blade has been tested in the 6- by 6-foot test section of the Langley stability tunnel to determine if the aerodynamic characteristics were seriously affected by cross flow or fabric distortion. The outer portion of the blade was tested as a reflection plane model pivoted about the tunnel wall to obtain various angles of cross flow over the blade. Because the tunnel wall acts as a plane of symmetry, the measured aerodynamic characteristics correspond to those of an airfoil having various angles of sweepforward and sweepback. Tests were made with the vents on the lower surface open and also with the vents sealed and the internal pressure held at -20 inches of water producing an internal pressure coefficient of -1.059.

The change in contour resulting from the range of internal pressures used had very little effect on the aerodynamic characteristics of the blade. The test methods were considered to simulate inadequately the flow conditions over the rotor blade because the effects of cross flow were limited to conditions corresponding to sweep of the blade. The results indicated that this type of cross flow had only minor effects on the aerodynamic characteristics of the blade. It is believed, therefore, that future tests to determine the effects on the aerodynamic characteristics of cross flow should utilize complete rotors.

## INTRODUCTION

An investigation of the rotor of the PV-2 helicopter has been made in the Langley full-scale tunnel (reference 1). In connection with these tests, the Bureau of Aeronautics requested wind-tunnel tests to investigate the effects of cross flow and fabric distortion on the aerodynamic characteristics of the rotor blade. A portion of a PV-2 helicopter rotor blade was installed as a reflection plane model in the 6- by 6-foot test section of the Langley stability tunnel for the tests. Inasmuch as the tunnel wall acted as a plane of symmetry, pivoting the blade forward and backward produced the same aerodynamic effects as changing the angle of sweep of an airfoil, the semispan of which is represented by the blade under test. It is realized that this method of test does not simulate the operating conditions of an actual rotor blade. It was believed, however, that results from this test installation would indicate qualitatively any important changes in aerodynamic characteristics caused by cross flow and surface distortion.

At sweep angles varying from  $30^\circ$  forward to  $30^\circ$  backward, a range of pitch angles from  $0^\circ$  to the stall was covered. Tests were made with two conditions of internal pressure. Measurements were made of the lift, drag, and pitching moment about the spar axis. The profile drag was measured by means of wake surveys behind one panel of the blade. The deflection of the fabric along the center line of this panel was determined. By means of tufts mounted on the blade surface, studies were made of the stalling characteristics near the tip.

## COEFFICIENTS AND SYMBOLS

$C_L$	lift coefficient, $L/qS$
$C_D$	drag coefficient, $D/qS$
$C_{m_s}$	pitching-moment coefficient about spar axis, $M/qSc$
$P_i$	internal pressure coefficient, $p_i/q$
$c_l$	section lift coefficient, assumed equal to $C_L$

- $c_{de}$  effective section drag coefficient,  $C_D - \frac{C_L^2}{\pi Au}$
- $c_{m_c/4}$  pitching-moment coefficient about quarter-chord line,  $C_{m_s} + 0.063C_L$
- $c_d$  section drag coefficient from wake surveys,

$$\frac{2}{c} \int_{\text{wake}} \sqrt{\frac{H_w - p_w}{H_o - p_o}} \left( 1 - \sqrt{\frac{H_w - p_o}{H_o - p_o}} \right) dz$$

where

- $q$  dynamic pressure,  $\frac{1}{2}\rho v^2$
- $S$  nominal blade area, equal to area at zero sweep angle
- $c$  chord of uniform section of blade
- $p_i$  internal pressure relative to free-stream static pressure
- $A$  aspect ratio
- $f$  induced angle-of-attack factor (from reference 2)
- $u$  induced drag factor (from reference 2)
- $H_w$  local total head in wake
- $p_w$  local static pressure in wake
- $H_o$  free-stream total head
- $p_o$  free-stream static pressure
- $z$  vertical distance in wake
- and
- $\theta$  pitch angle, measured about spar axis
- $\gamma$  angle of sweep, positive when tip is forward

- $\theta_0$  section pitch angle,  $f\theta = \frac{57.3C_L}{\pi A \cos \gamma}$   
 $\alpha_0$  section angle of attack,  $\theta_0 \cos \gamma$   
 $\rho$  mass density of air  
 $V$  free-stream velocity  
 $x$  chordwise distance from leading edge  
 $d$  fabric deflection from wind-off position  
 $m$  mean camber  
 $x_{ac}$  chordwise location of aerodynamic center

#### DESCRIPTION OF MODEL

The rotor blade tested was furnished by the PV Engineering Forum and was constructed similarly to the production PV-2 blades except that the usual tubular spar was replaced by a solid steel spar to reduce deflections of the blade during tunnel tests. The fabric covering was finished by the production process which produced a very smooth finish; no fabric grain could be felt or seen. The fabric surface between ribs, however, departed somewhat from the NACA 0012.6 airfoil shape of the ribs.

Before the tunnel tests, the blade structure was cut away from the spar over the inboard portion leaving the outer 59 inches intact. The exposed spar at the inboard end was passed through the tunnel wall and was mounted in bearings to support the blade on the balance system. An additional bearing was mounted in the blade at the tip end of the spar and was supported by two wires from the balances below the blade and by a counterweighted wire above the blade. Holes were drilled in each rib so that the internal pressure would be equalized throughout the blade. Details of the blade as tested are shown in figure 1.

During the tests, the sweep angle was changed by relocating the bearing supporting the inboard end of the spar. The counterweighted wire above the blade tip was

kept vertical. At each sweep angle used, the blade contour was extended by a steel skirt to within  $1/8$  inch of the tunnel wall. A photograph of the blade mounted in the tunnel is shown in figure 2.

#### APPARATUS AND TESTS

The tests were conducted in the 6- by 6-foot test section of the Langley stability tunnel. Most of the tests were made at a dynamic pressure  $q$  of 98.3 pounds per square foot, corresponding to a test Reynolds number of about 1,500,000 with a turbulence factor less than 1.04. Force measurements at zero sweep with vents open were also made at values of  $q$  of 24.9 and 64.3 pounds per square foot. It was observed that the blade was subjected to a violent shaking when it was stalled at the high tunnel speeds; consequently no tests were made beyond the stall except at low tunnel speeds. The lift and drag of the blade were measured by the tunnel balance system and the pitching moment about the spar axis was measured by means of a spring torque balance. During the tests with negative internal pressure the vent holes on the blade were sealed and a suction pump was used to maintain the negative pressure. The fabric deflection in panel 5 was measured photographically by the method described in reference 3. Measurements of the initial fabric tension, however, could not be made because of the curvature of the fabric.

While the blade was being prepared for the tests, it was observed that the fabric covering began to separate from one of the ribs at a positive internal pressure of about 8 inches of water. Consequently, no tests were run using positive internal pressure because of the possibility of damaging the blade.

The profile-drag measurements were made by means of a rake of total head and static tubes located in the wake of the blade. The tubes were connected to a multiple manometer which was photographed to record the pressures in the wake. For most of the wake surveys, the rake was located about one chord length downstream of the blade trailing edge so that the effects of any local irregularities on the blade surface would be minimized. One series of wake surveys, however, was made with the rake about  $1/10$  chord from the trailing edge to determine the effect of the ribs on the profile-drag coefficient.

It is estimated that the accuracy of the measurements was such as to give the following limits of error:

$\theta$ . . . . .	$\pm 0.2^\circ$	$c_d$ . . . . .	$\pm 0.0003$
$\gamma$ . . . . .	$\pm 0.2^\circ$	$C_{m_s}$ . . . . .	$\pm 0.001$
$C_L$ . . . . .	$\pm 0.01$	$P_1$ . . . . .	$\pm 0.003$
$C_D$ . . . . .	$\pm 0.001$		

The stalling characteristics near the blade tip were recorded by photographing wool tufts fastened to the upper surface of the blade. These tests were made at a reduced tunnel speed corresponding to a Reynolds number of about 500,000 to reduce the violence of the shaking above the stall. During the tuft observations, the upper tip support wire was removed and its point of attachment on the upper surface was faired smooth.

The following jet-boundary corrections have been applied:

$$\Delta\theta = \frac{0.63C_L}{\cos \gamma}$$

$$\Delta C_D = 0.0093C_L^2$$

These corrections were derived for the condition of zero sweep angle but were used at all sweep angles. The jet-boundary correction to pitching moment was found to be negligible.

Inspection of the force test results showed a random variation in minimum drag coefficient for the various sweep and internal pressure conditions. Because the upper tip support wire bowed rearward under air load, it was necessary to move the upper end of the wire between the wind-off and wind-on conditions to prevent fouling against the tunnel ceiling. The observed variation in minimum drag coefficient was probably caused mainly by the shift in the wind-off drag reading which occurred when the wire was moved. Because the magnitude of this

shift was not known, a constant increment was added to the drag coefficients of each test of such a value that the minimum drag agreed with that obtained from the wake surveys. Data presented in reference 4 show that this agreement should exist for high aspect-ratio airfoils with rounded tips at zero sweep.

## RESULTS AND DISCUSSION

The fabric deflections and resulting mean camber lines at the midspan of panel 5 are presented in figure 3 for a sweep angle of zero. Inspection of the fabric deflection data showed that changing the sweep angle had practically no effect on the fabric deflections. The curves of figure 3 show that at  $\theta = 0$ , with the vents open, both surfaces were slightly bulged. At positive values of  $\theta$  the upper surface bulged more and the lower surface tended to deflect inward so that a camber was produced which increased with increasing  $\theta$ . With an internal pressure coefficient of  $-1.059$ , large inward deflections of both surfaces were observed and the change in camber with  $\theta$  was less than with the vents open. The change in the airfoil section contour produced by fabric deflection is shown in figure 4 for several test conditions.

The aerodynamic characteristics of the portion of the blade tested are presented for the various test conditions in figures 5 to 14. The force and moment coefficients are based on the nominal area, that is, the blade area at zero sweep angle. The areas added by the blade-root extensions at sweep angles other than zero are given in table I. The data have been converted to the form of section characteristics which are presented in figures 15 to 23. Values of  $c_d$  obtained from wake surveys are also presented. The two values given for each lift coefficient were obtained from wake surveys at two spanwise stations, behind rib E and behind the center of panel 5.

Inspection of the data of figures 5 to 13 shows that with a highly negative internal pressure ( $P_i = -1.059$ ),  $C_L$  and  $C_{m_s}$  had a practically linear variation with  $\theta$  except for some rounding near the

stall. With the vents open, the lift coefficient and the pitching-moment coefficient show a slight change from the linear variation with pitch angle observed with  $P_1 = -1.059$  over a range of pitch angles from  $8^\circ$  to  $12^\circ$ . In the same range of pitch angles,  $P_1$  reached a positive peak with the vents open.

The effect on the aerodynamic characteristics of varying the dynamic pressure  $q$  is shown by figure 14. For small values of  $\theta$ , decreasing  $q$  had a negligible effect although the maximum positive value of  $P_1$  produced by the vents was increased considerably by decreasing  $q$ . At large values of  $\theta$ , the decrease in lift coefficient and stalling angle with decreasing  $q$  follow the expected variation with Reynolds number.

The tunnel data were reduced to the form of section characteristics by means of the equations derived from lifting line theory and given under definitions of symbols. Values of the plan-form correction factors  $f$  and  $u$  were determined from charts given in reference 2 for the aspect ratio corresponding to each sweep angle. The values of aspect ratio  $f$  and  $u$  used in the computations are given in table I. Because conversion of the present data to infinite aspect ratio was based on the induced effects at zero sweep, the section characteristics presented for sweep angles other than zero retain the incremental induced effects caused by the sweep angle. The difference between the values of  $c_d$  and  $c_{d_e}$  at lift coefficients greater than zero (figs. 15 to 23) is similar to that observed in previous experiments (reference 4) but is further influenced in the present tests by the induced effects of the gap at the tunnel wall and the change in induced drag and jet-boundary correction with sweep angle.

The variation of  $c_d \cos \gamma$  with sweep angle is presented in figure 24. Because the values of  $c_d$  were based on a constant blade chord and the chord measured in the direction of the air stream increases with sweep angle, the value of  $c_d \cos \gamma$  represents the drag of a unit span of blade measured along the blade axis at any sweep angle. The curves of figure 24 indicate that the negative internal pressure increased the drag by an increment which was practically constant with sweep angle. If angle of sweep were to increase the drag by

producing cross flow over the blade ribs, it would be expected that the curves representing the two internal pressure conditions would diverge with sweep. It may be concluded, therefore, that no such effect existed. The small asymmetry observed at the higher lift coefficient is probably associated with the location of the survey rake in that it measured the wake from different portions of the blade when swept forward and backward, respectively. The difference between the two values of  $c_d$  obtained at a given lift coefficient (figs. 15 to 23) indicates that the measured drag may be sensitive to small changes in rake location at the higher lift coefficients.

The effective profile-drag coefficients  $c_{de}$  (figs. 15 to 23) also indicate that cross flow over the blade ribs was not instrumental in increasing the profile drag because no increase with sweep of the increment of  $c_{de}$  caused by an internal pressure change was observed. The values of  $c_{de}$  do, however, increase with sweep, especially with sweepforward, but the variation of  $c_{de}$  with sweep is to be considered a change in induced drag including the effects of variation with sweep of the effective tip shape and the jet-boundary corrections. The variation of  $c_{de}$  with sweep must, therefore, be considered a function of this particular test arrangement and does not represent a change in blade profile-drag coefficient with sweep.

The variation of section drag coefficient across one fabric panel (panel 5) is shown in figure 25 for zero sweep and pitch angles and for the two internal pressure conditions. The data were obtained from wake surveys made at a station about 1/10 chord behind the trailing edge. The section drag with the vents open is essentially unaffected by the ribs; the drag behind the ribs being practically the same as that behind the panel center. A very slight increase in drag behind the ribs is observed for the negative internal pressure condition.

The variation in  $\partial c_l / \partial \alpha_0$  with sweep angle for the two conditions of internal pressure is shown in figure 26. The values of  $\partial c_l / \partial \alpha_0$  were obtained by dividing the values of  $\partial c_l / \partial \theta_0$  measured from figures 15 through 23

by  $\cos \gamma$ . At large sweep angles, some reduction in  $\partial c_l / \partial \alpha_0$  occurred. The variation shown is subject to the same limitations as were discussed in connection with the effective profile-drag coefficient and must, therefore, be considered a function of the particular test arrangement used. Comparison of the two internal pressure conditions, however, is not subject to these limitations and indicates that fabric distortion had practically no effect on the lift-curve slope.

The effect of sweep angle on the aerodynamic-center location is also shown in figure 26 for the two internal pressure conditions. The aerodynamic center was always located between 23 and 24 percent of the blade chord and was not appreciably affected by variation of sweep angle or internal pressure.

The results of the stall studies are shown in figure 27 in which diagrams of the stall patterns obtained over the outer three-fifths of the portion of the blade tested are presented. With no sweep, the blade showed a tendency to stall at the inboard end first with the stall progressing toward the tip as the angle of attack was increased. Sweeping the blade forward delayed the tip stall to very high values of pitch angle whereas sweepback caused the tip region to stall first. The direction of flow on the upper surface is indicated by arrows on the diagram. As would be expected, the boundary layer was carried inward along the trailing edge for the sweepforward conditions, and outward for the sweepback conditions. The stall patterns obtained are affected to some extent by tunnel-wall interference and its variation with sweep angle. On a rotating blade, the stall patterns would be modified by a number of effects, some of which are the variation of Reynolds number along the blade, the action of centrifugal force on the boundary layer, and changes in spanwise distribution of load over the blade.

#### CONCLUDING REMARKS

The change in contour resulting from the range of internal pressures used had very little effect on the aerodynamic characteristics of the blade. The test methods were considered to simulate inadequately the flow conditions over the rotor blade because the effects of cross flow were limited to conditions corresponding

to sweep of the blade. The results indicated that this type of cross flow had only minor effects on the aerodynamic characteristics of the blade. It is believed, therefore, that future tests to determine the effects on the aerodynamic characteristics of cross flow should utilize complete rotors.

Langley Memorial Aeronautical Laboratory  
National Advisory Committee for Aeronautics  
Langley Field, Va.

*William B. Kemp, Jr.*

William B. Kemp, Jr.  
Aeronautical Engineer

Approved:

*Hartley A. Soule*  
Hartley A. Soule

Chief of Stability Research Division

MWD

## REFERENCES

1. Migotsky, Eugene: Full-Scale Tunnel Performance Tests of the PV-2 Helicopter Rotor. NACA MR No. L5C29a, Bur. Aero., 1945.
2. Anderson, Raymond F.: Determination of the Characteristics of Tapered Wings. NACA Rep. No. 572, 1936.
3. Neihouse, A. I., and Kemp, W. B.: The Effect of Fabric Deflection on Rudder Hinge-Moment Characteristics as Determined by Tests in the Stability Tunnel. NACA RMR No. L4J20, Bur. Aero., 1944.
4. Goett, Harry J., and Bullivant, W. Kenneth: Tests of NACA 0009, 0012, and 0018 Airfoils in the Full-Scale Tunnel. NACA Rep. No. 647, 1938.

TABLE I

Sweep angle, $\gamma$ (deg)	Root fairing area (sq ft)	Aspect ratio A	Induced angle factor, f	Induced drag factor, u
0	0	12.82	0.983	0.926
5	.026	12.77	.983	.926
10	.053	12.54	.983	.928
20	.110	11.52	.984	.935
30	.175	9.87	.984	.948
-5	.027	12.95	.983	.925
-10	.055	12.88	.983	.926
-20	.113	12.19	.983	.931
-30	.179	10.78	.984	.941

NATIONAL ADVISORY  
COMMITTEE FOR AERONAUTICS

FIGURE LEGENDS

- Figure 1.- Dimensions of PV-2 helicopter rotor blade as tested.
- Figure 2.- Photograph of PV-2 helicopter rotor blade mounted in tunnel at a sweep angle of  $30^{\circ}$ .
- Figure 3.- Fabric deflection and mean camber at midspan of panel 5 of PV-2 helicopter rotor blade,  $\gamma = 0^{\circ}$ ,  $q = 98.3$  lb/sq ft.
- Figure 4.- Contours of blade section at midspan of panel 5 of PV-2 helicopter rotor blade,  $\gamma = 0$ ,  $q = 98.3$  lb/sq ft.
- Figure 5.- Aerodynamic characteristics of outer portion of PV-2 helicopter rotor blade,  $\gamma = 0^{\circ}$ .
- Figure 6.- Aerodynamic characteristics of outer portion of PV-2 helicopter rotor blade,  $\gamma = 5^{\circ}$ .
- Figure 7.- Aerodynamic characteristics of outer portion of PV-2 helicopter rotor blade,  $\gamma = 10^{\circ}$ .
- Figure 8.- Aerodynamic characteristics of outer portion of PV-2 helicopter rotor blade,  $\gamma = 20^{\circ}$ .
- Figure 9.- Aerodynamic characteristics of outer portion of PV-2 helicopter rotor blade,  $\gamma = 30^{\circ}$ .
- Figure 10.- Aerodynamic characteristics of outer portion of PV-2 helicopter rotor blade,  $\gamma = 5^{\circ}$ .
- Figure 11.- Aerodynamic characteristics of outer portion of PV-2 helicopter rotor blade,  $\gamma = -10^{\circ}$ .
- Figure 12.- Aerodynamic characteristics of outer portion of PV-2 helicopter rotor blade,  $\gamma = -20^{\circ}$ .
- Figure 13.- Aerodynamic characteristics of outer portion of PV-2 helicopter rotor blade,  $\gamma = -30^{\circ}$ .
- Figure 14.- Effect of dynamic pressure on the aerodynamic characteristics of the outer portion of PV-2 helicopter rotor blade, vents open.

## FIGURE LEGENDS - Concluded

Figure 15.- Section characteristics of the outer portion of PV-2 helicopter rotor blade,  $\gamma = 0^\circ$ .

Figure 16.- Section characteristics of the outer portion of PV-2 helicopter rotor blade,  $\gamma = 5^\circ$ .

Figure 17.- Section characteristics of the outer portion of PV-2 helicopter rotor blade,  $\gamma = 10^\circ$ .

Figure 18.- Section characteristics of the outer portion of PV-2 helicopter rotor blade,  $\gamma = 20^\circ$ .

Figure 19.- Section characteristics of the outer portion of PV-2 helicopter rotor blade,  $\gamma = 30^\circ$ .

Figure 20.- Section characteristics of the outer portion of PV-2 helicopter rotor blade,  $\gamma = -5^\circ$ .

Figure 21.- Section characteristics of the outer portion of PV-2 helicopter rotor blade,  $\gamma = -10^\circ$ .

Figure 22.- Section characteristics of the outer portion of PV-2 helicopter rotor blade,  $\gamma = -20^\circ$ .

Figure 23.- Section characteristics of the outer portion of PV-2 helicopter rotor blade,  $\gamma = -30^\circ$ .

Figure 24.- Variation of  $c_d \cos \gamma$  with sweep angle.

Figure 25.- Variation of section drag coefficient across panel 5 (from wake surveys),  $\gamma = 0$ ,  $C_L = 0.015$ .

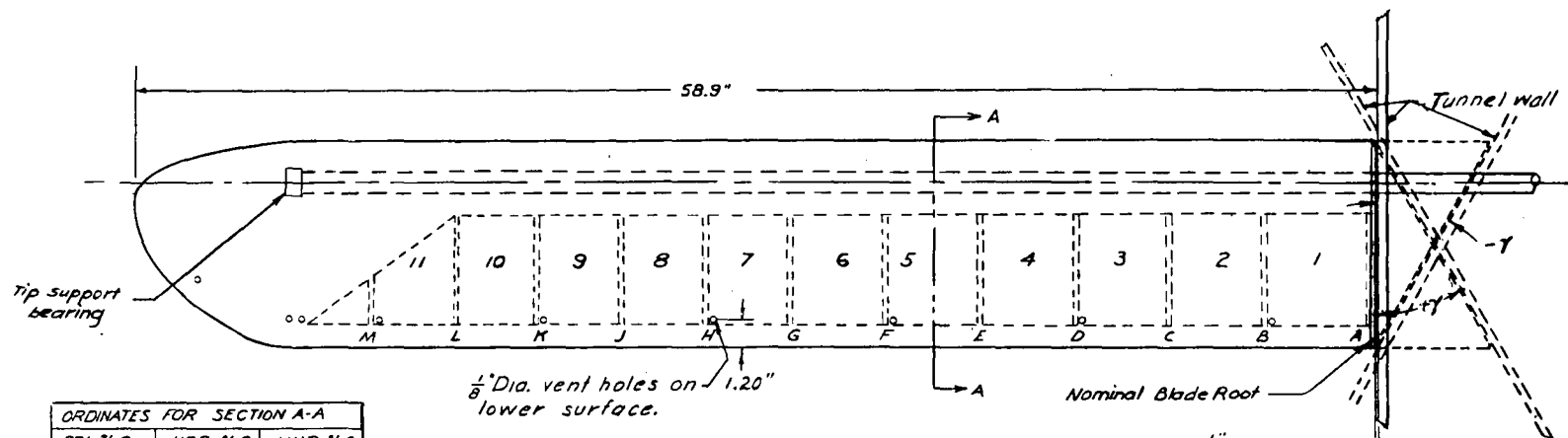
Figure 26.- Effect of sweep on  $\partial C_L / \partial \alpha_0$  and location of aerodynamic center.

Figure 27.- Stall progression over outer three-fifths of portion of PV-2 helicopter rotor blade tested.

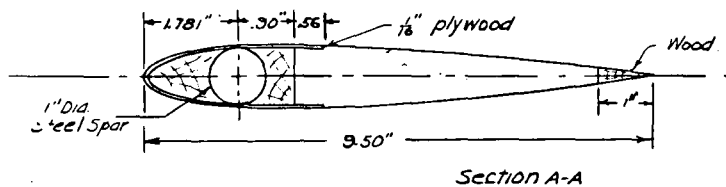
(a) Swept forward.

Figure 27.- (Concluded.)

(b) Swept back.



ORDINATES FOR SECTION A-A		
STA. %C.	UPR %C	LWR %C
0.00	0.00	0.00
1.04	1.79	1.84
2.09	2.48	2.51
4.19	3.41	3.50
7.33	4.34	4.38
9.55	4.91	4.97
15.70	5.68	5.71
20.90	6.04	6.09
26.20	6.25	6.30
31.40	6.24	6.25
36.60	6.07	6.04
47.20	5.49	5.45
57.70	4.76	4.70
68.10	3.85	3.79
78.60	2.84	2.76
89.00	1.76	1.64
94.9	1.11	0.96
100.00	0.26	0.22



Chord: 0.792 ft.  
 Span: 4.910 ft.  
 Area: 3.765 Sq.ft.  
 Airfoil section at ribs N.A.C.A 0012.6

Rib.	Dist. From NOMINAL ROOT
A	.25
B	5.25
C	9.75
D	14.25
E	18.75
F	23.25
G	27.75
H	31.75
J	35.75
K	39.75
L	43.75
M	47.75

NATIONAL ADVISORY COMMITTEE FOR AERONAUTICS.

Figure 1 - Dimensions of PV-2 helicopter rotor blade as tested.

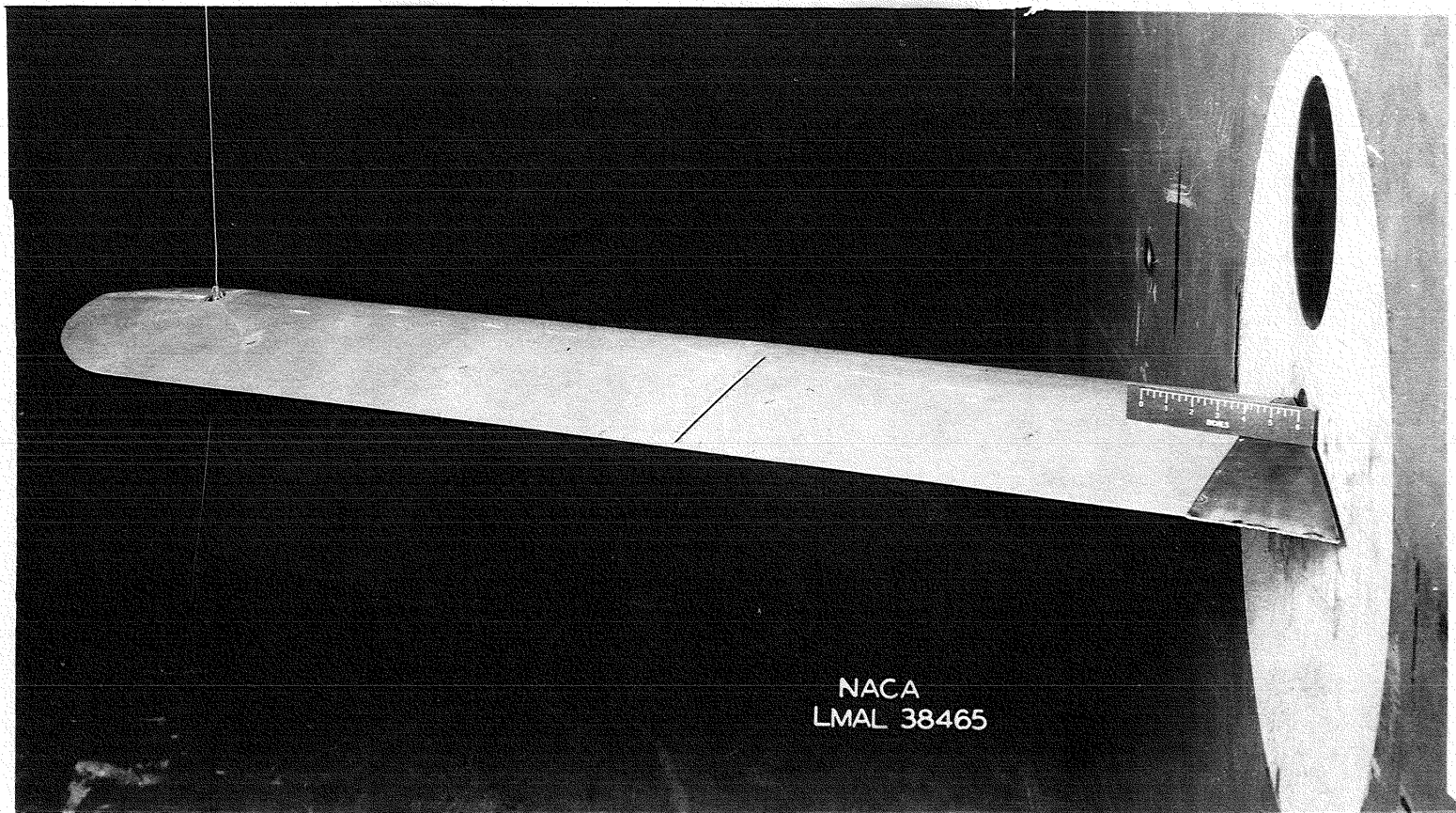


Figure 2.- Photograph of PV-2 helicopter rotor blade mounted in tunnel at a sweep angle of  $30^{\circ}$ .

NATIONAL ADVISORY COMMITTEE FOR AERONAUTICS  
LANGLEY MEMORIAL AERONAUTICAL LABORATORY - LANGLEY FIELD, VA.

NR No. 15C29b

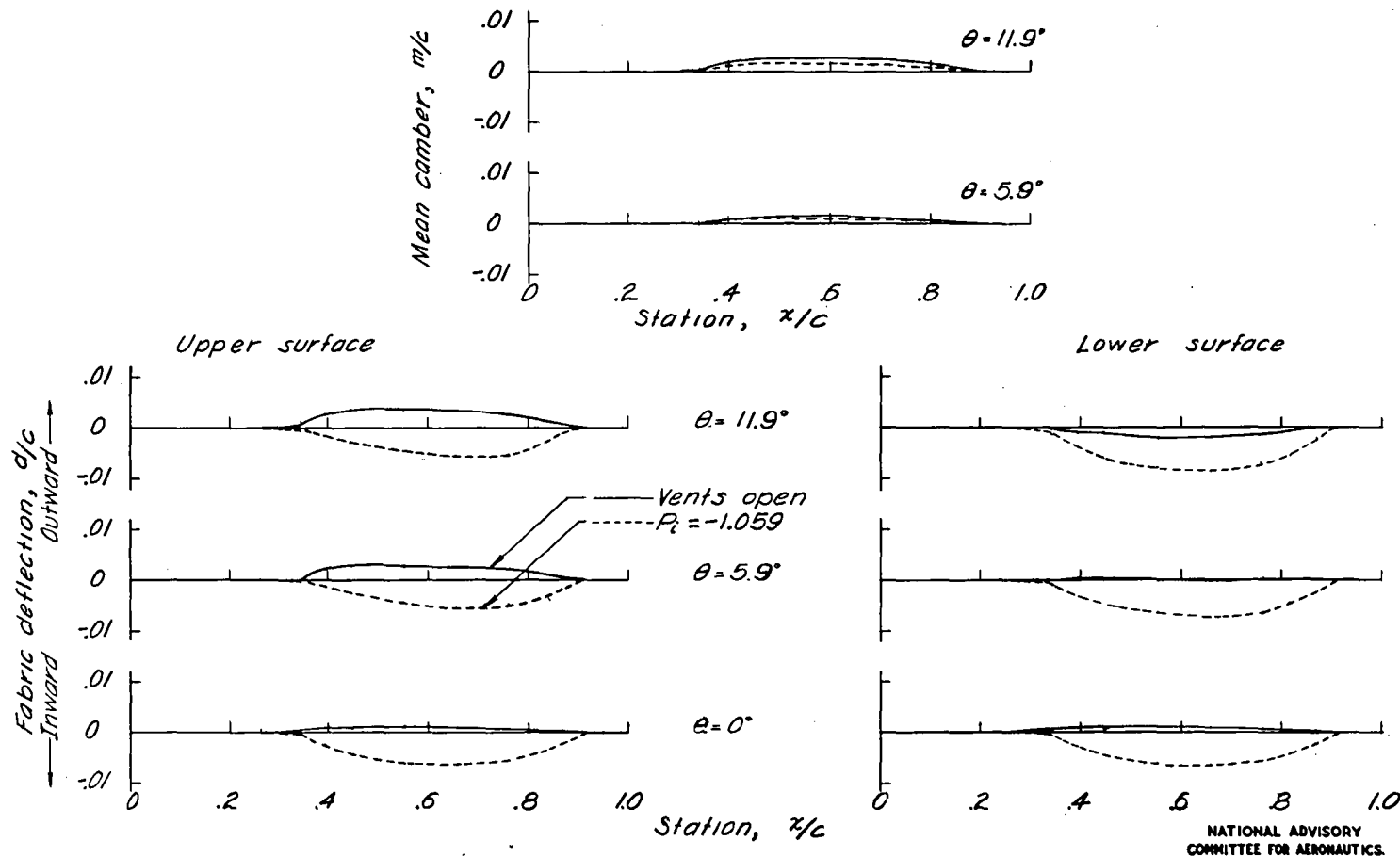
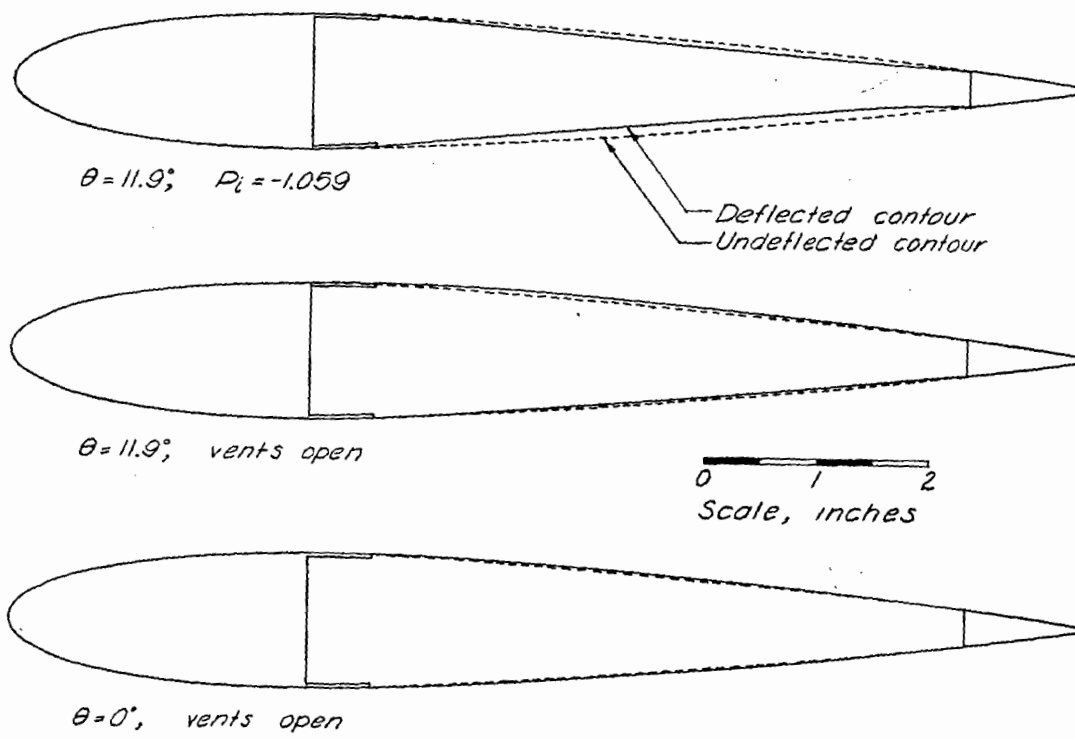


Figure 3 - Fabric deflection and mean camber at midspan of panel 5 of PV-2 helicopter rotor blade,  $\gamma = 0^\circ$ ,  $q = 98.3 \text{ lb/sq ft}$ .



NATIONAL ADVISORY  
COMMITTEE FOR AERONAUTICS.

Figure 4 - Contours of blade section at midspan of panel 5 of PV-2 helicopter rotor blade,  $\gamma = 0$ ,  $q = 98.3 \text{ lb/sq ft}$ .

MR No. L5C29b

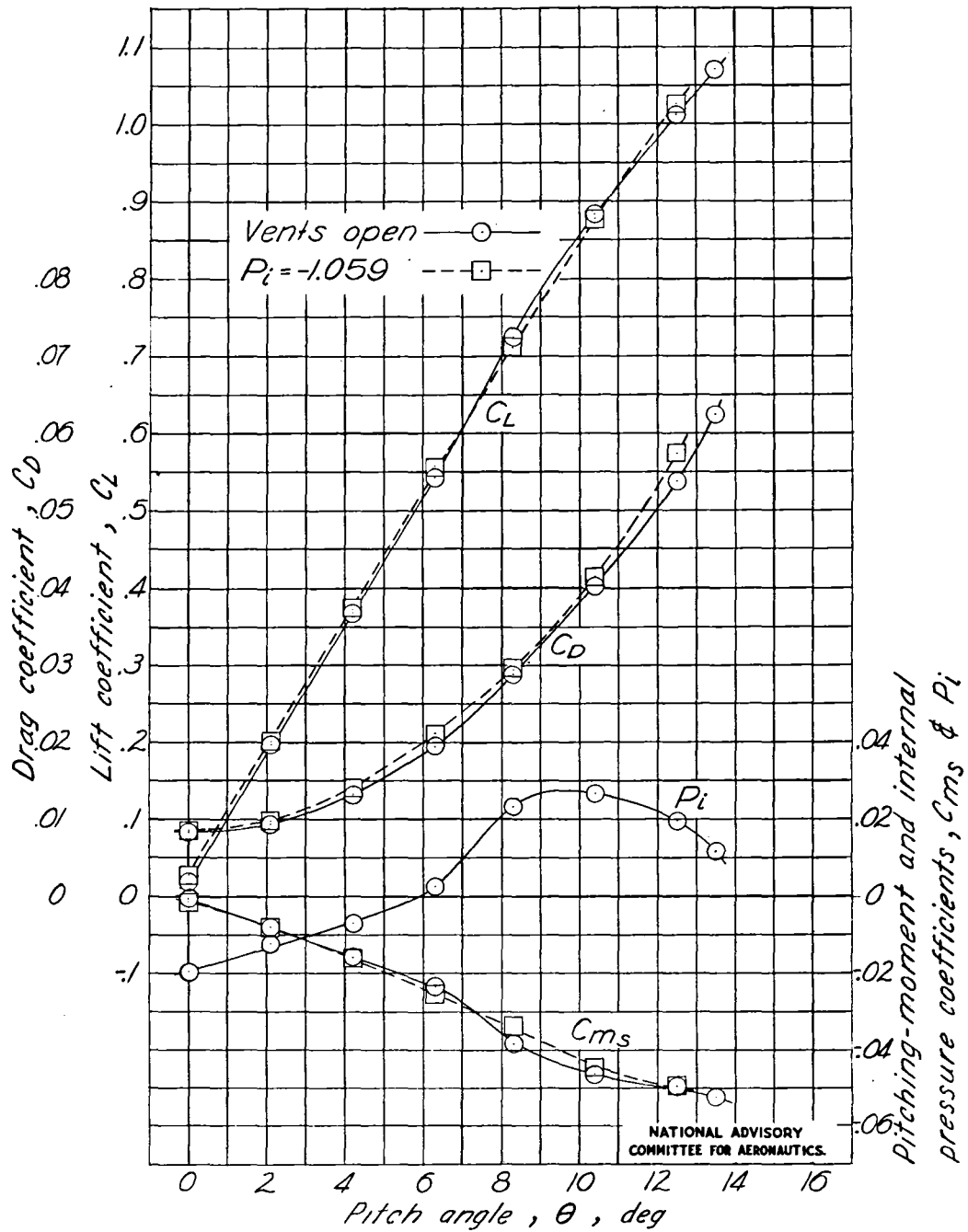


Figure 5.- Aerodynamic characteristics of outer portion of PV-2 helicopter rotor blade,  $\gamma = 0^\circ$ .

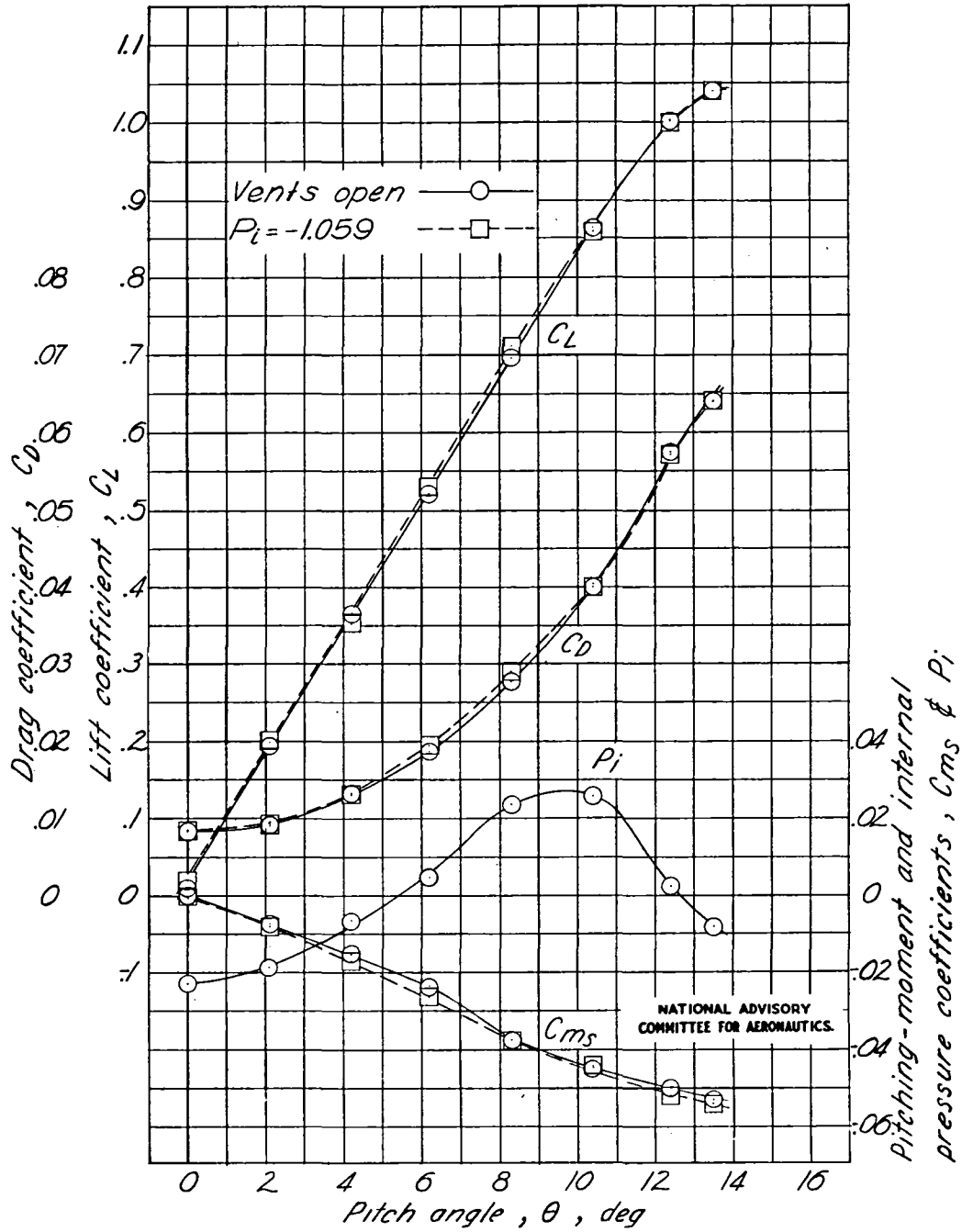


Figure 6 .- Aerodynamic characteristics of outer portion of PV-2 helicopter rotor blade ,  $\gamma = 5^\circ$

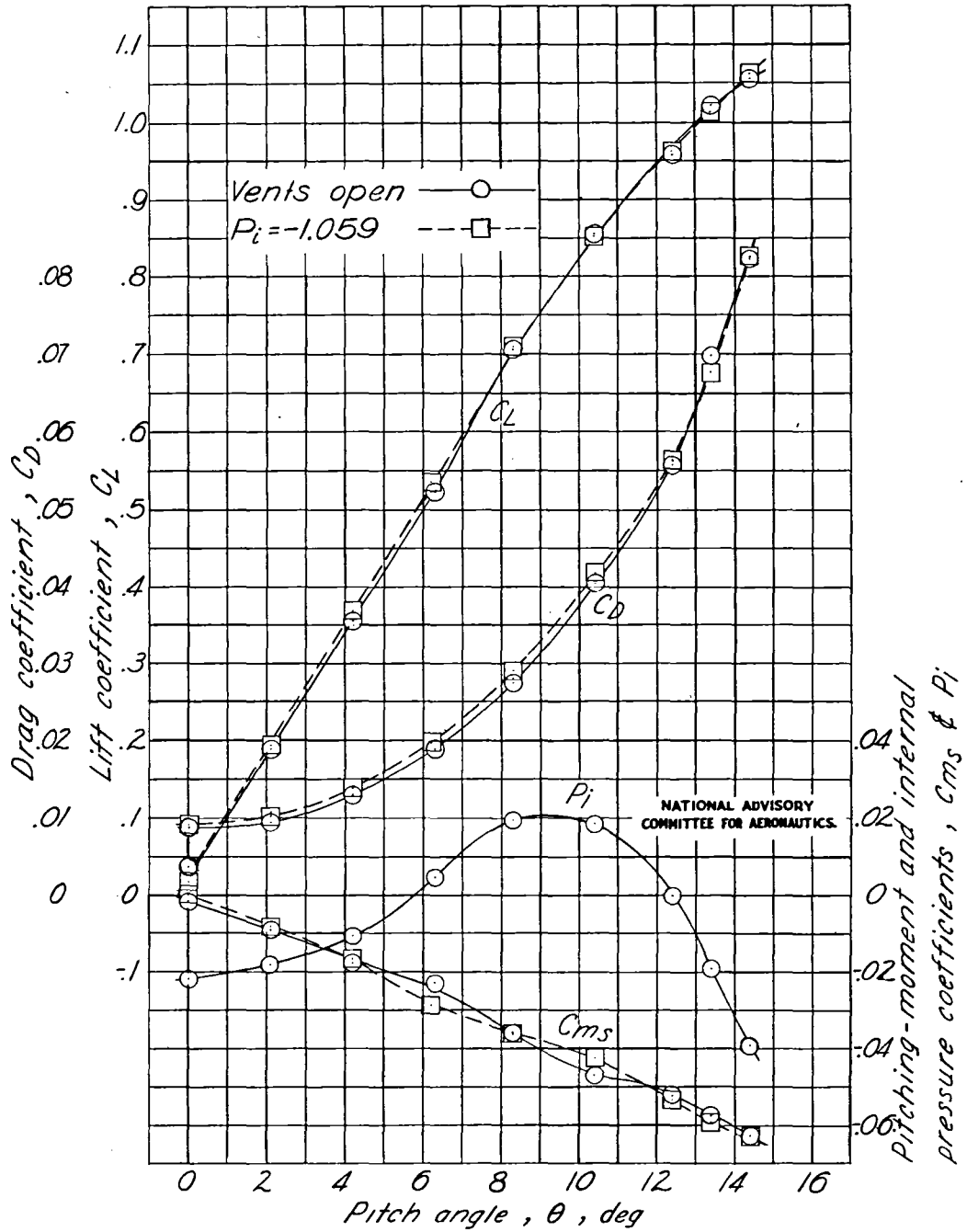


Figure 7.- Aerodynamic characteristics of outer portion of PV-2 helicopter rotor blade,  $\gamma = 10^\circ$ .

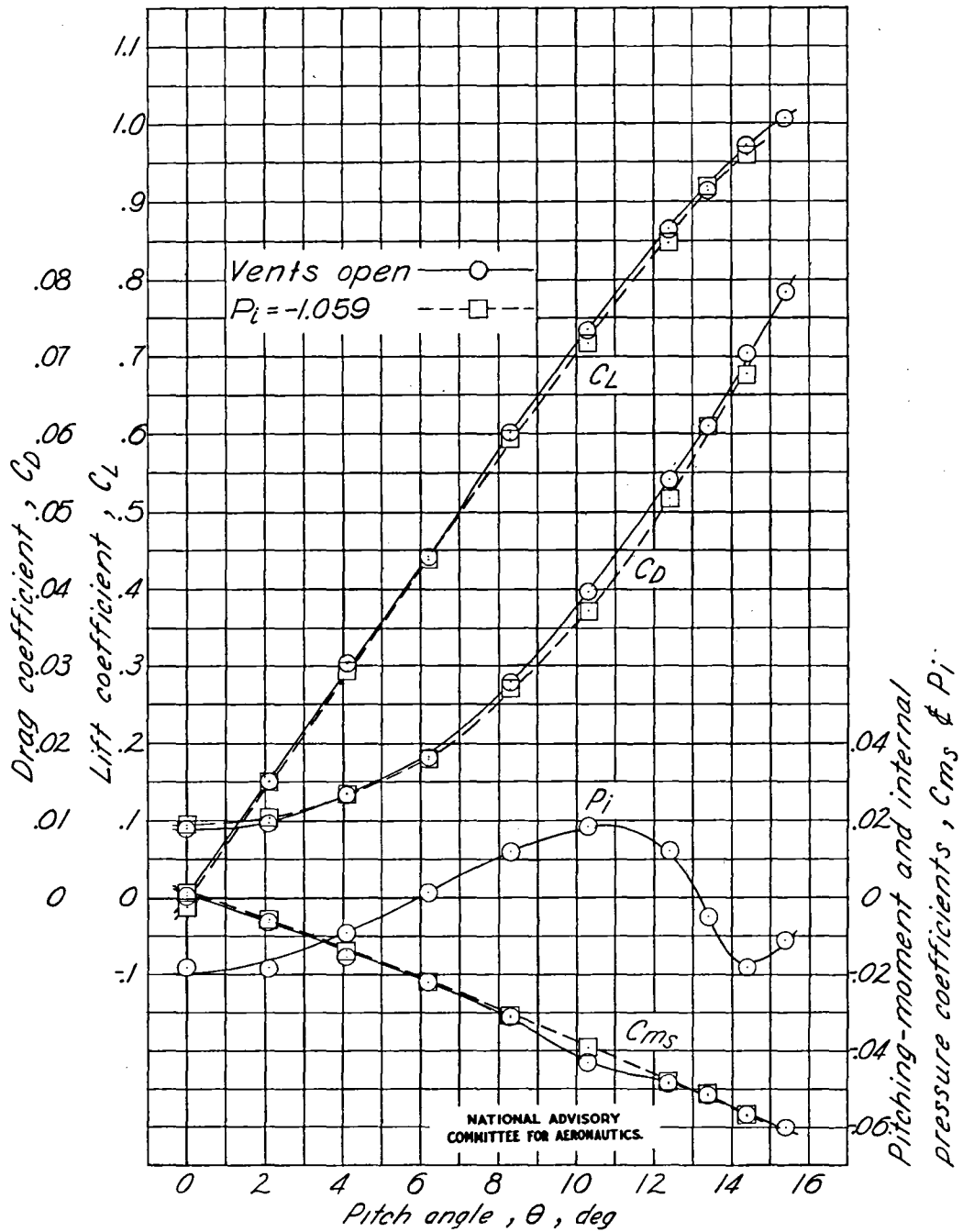


Figure 8 .- Aerodynamic characteristics of outer portion of PV-2 helicopter rotor blade,  $\gamma = 20^\circ$ .

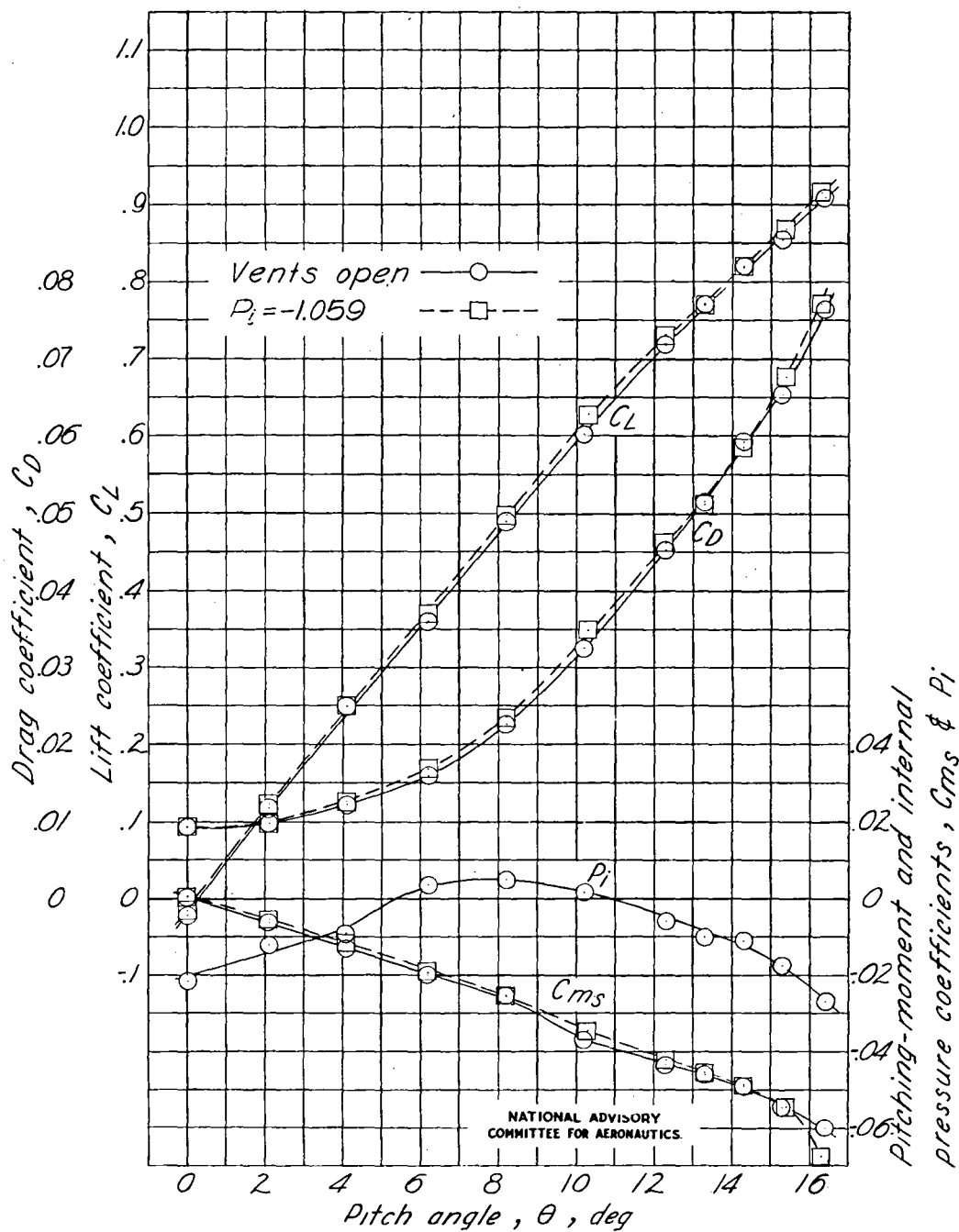


Figure 9.- Aerodynamic characteristics of outer portion of PV-2 helicopter rotor blade,  $\gamma = 30^\circ$ .

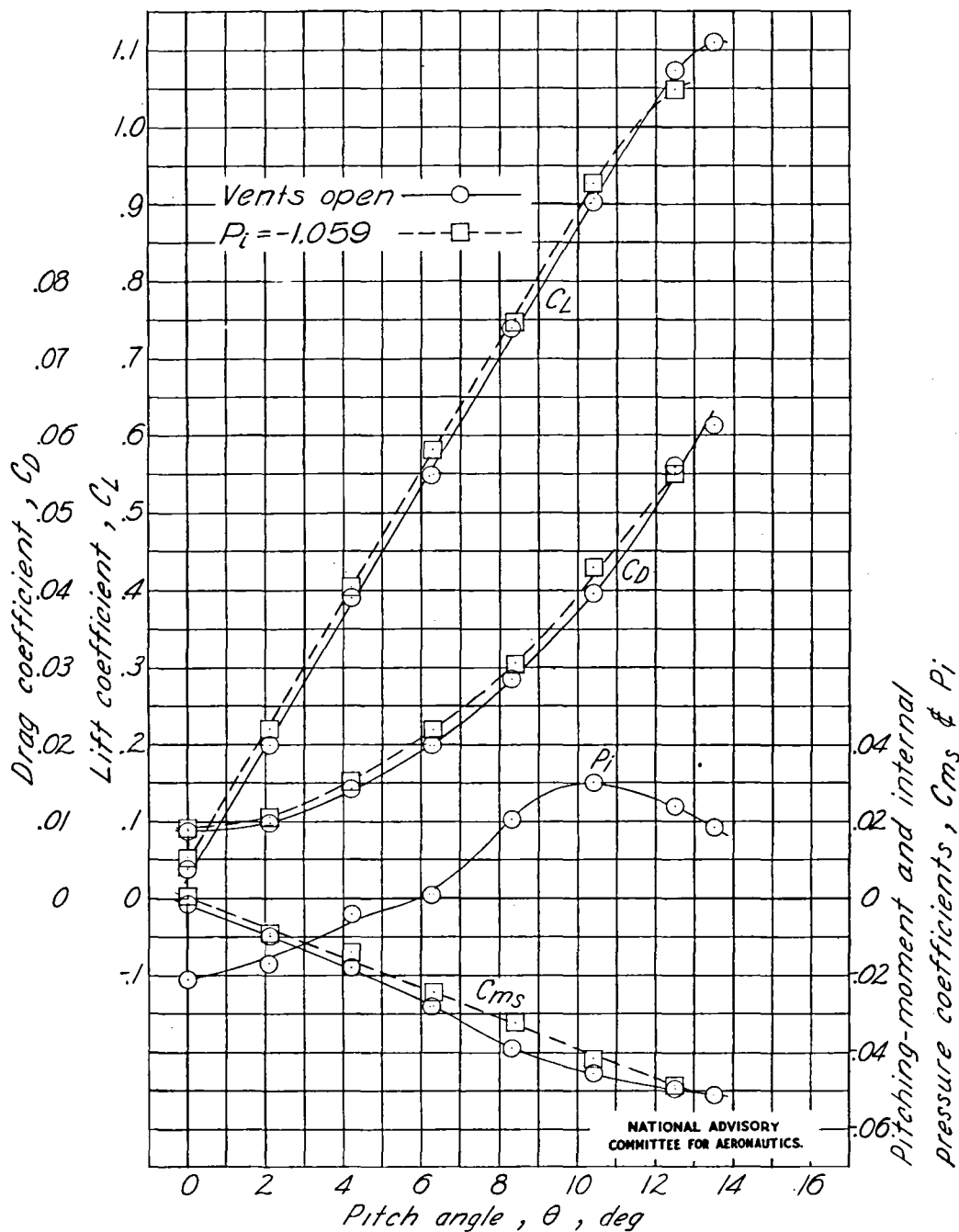


Figure 10.- Aerodynamic characteristics of outer portion of PV-2 helicopter rotor blade,  $\gamma = -5^\circ$ .

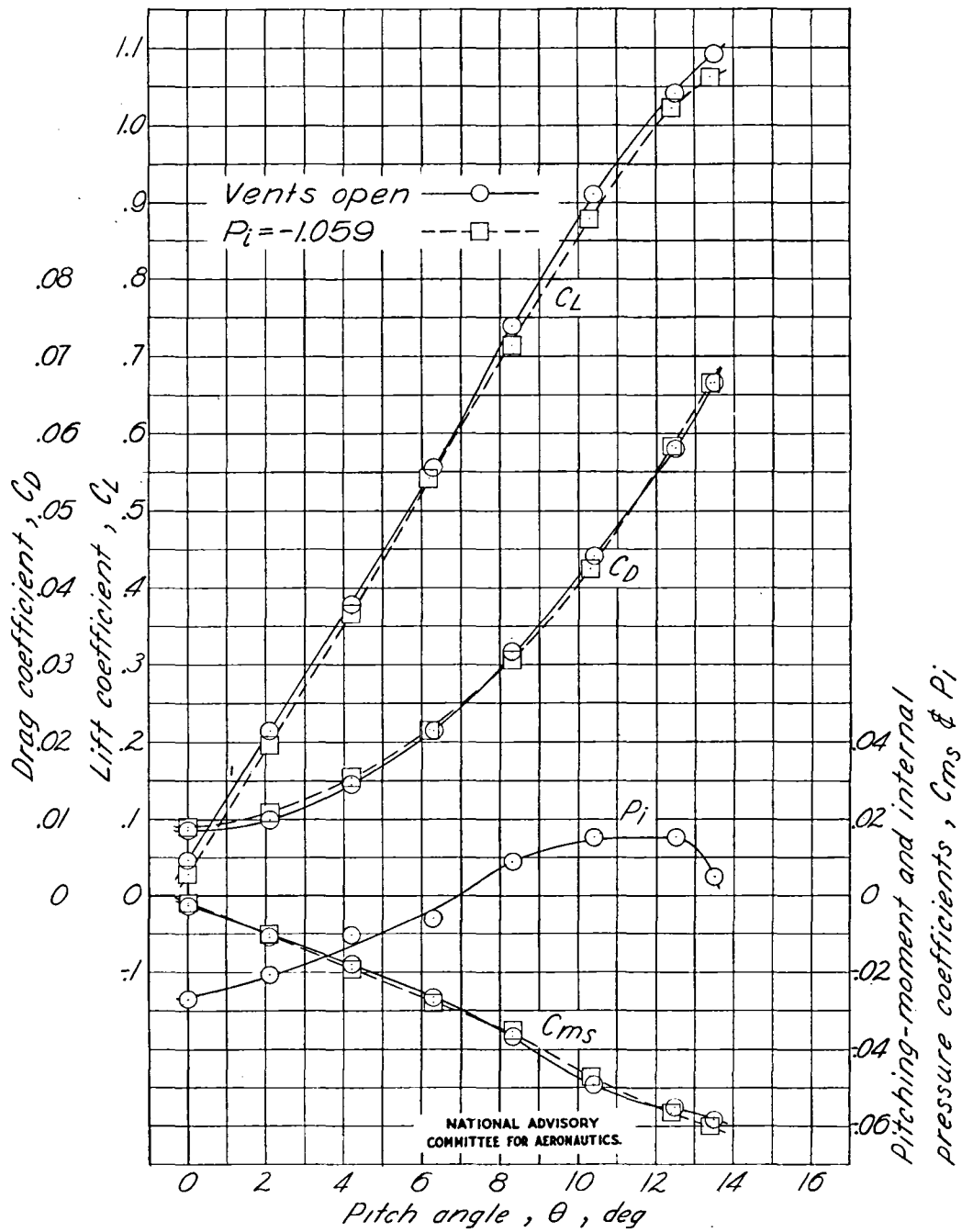


Figure 11.- Aerodynamic characteristics of outer portion of PV-2 helicopter rotor blade,  $\gamma = -10^\circ$ .

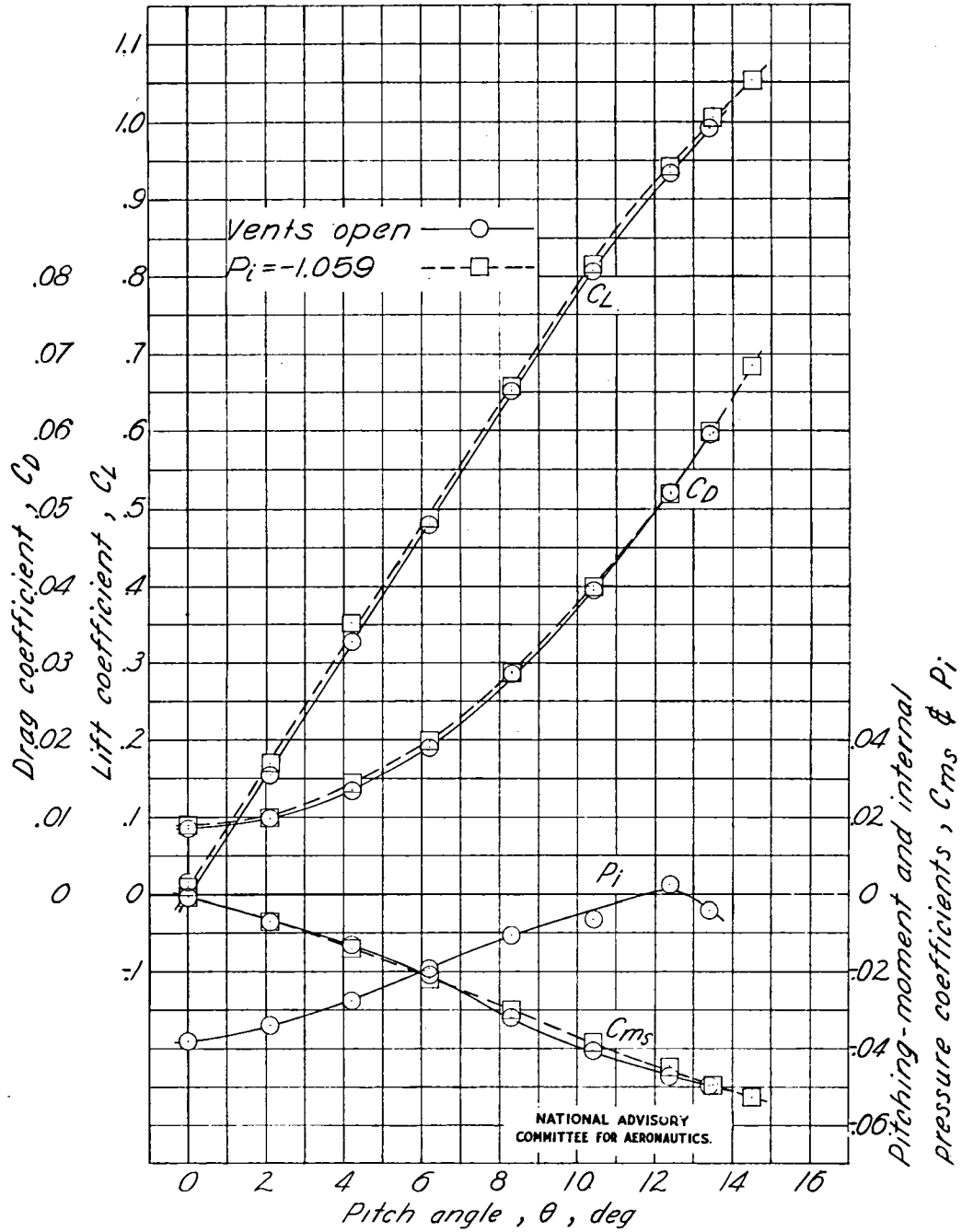


Figure 12.- Aerodynamic characteristics of outer portion of PV-2 helicopter rotor blade,  $\gamma = -20^\circ$ .

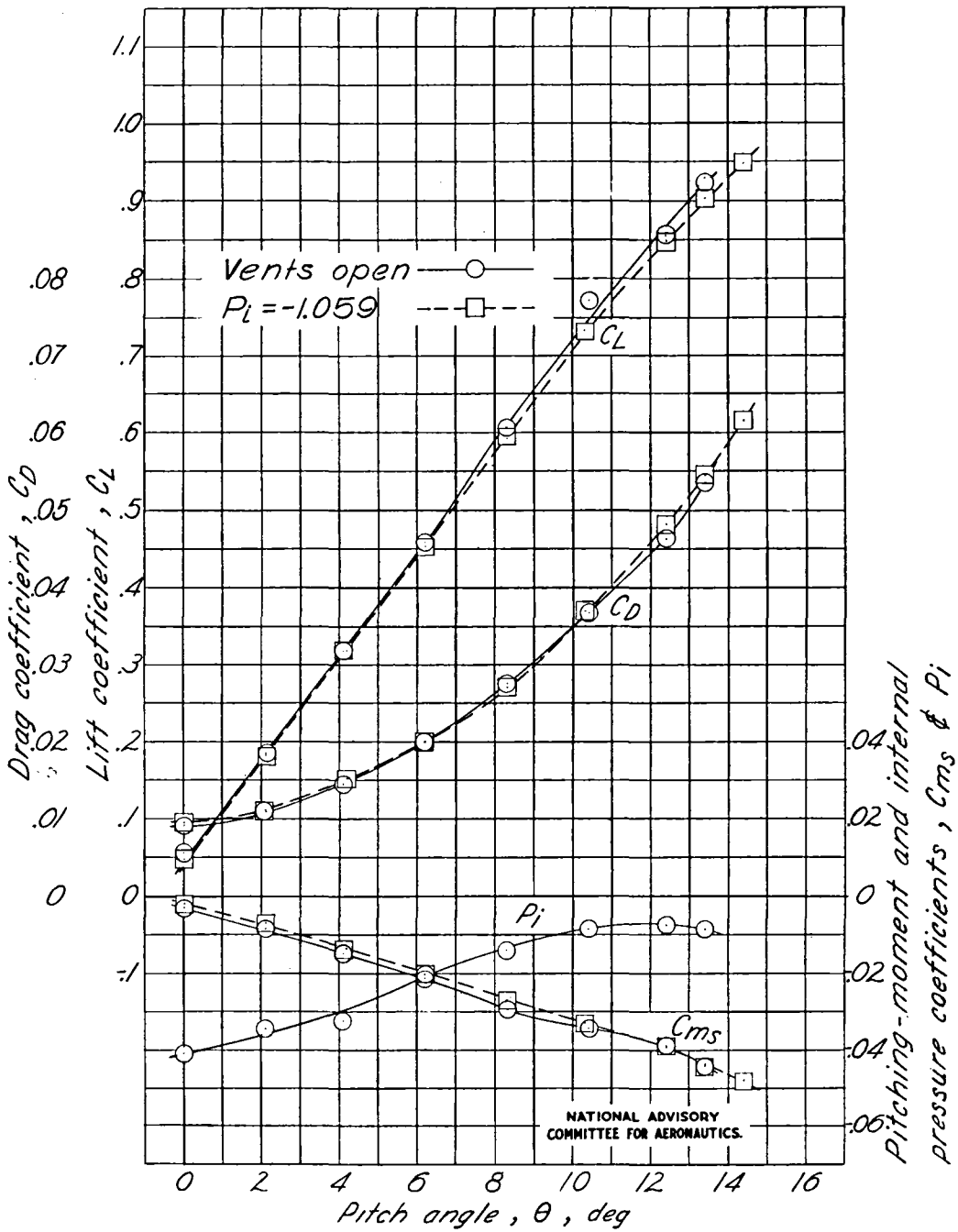


Figure 13.- Aerodynamic characteristics of outer portion of PV-2 helicopter rotor blade,  $\gamma = -30^\circ$ .

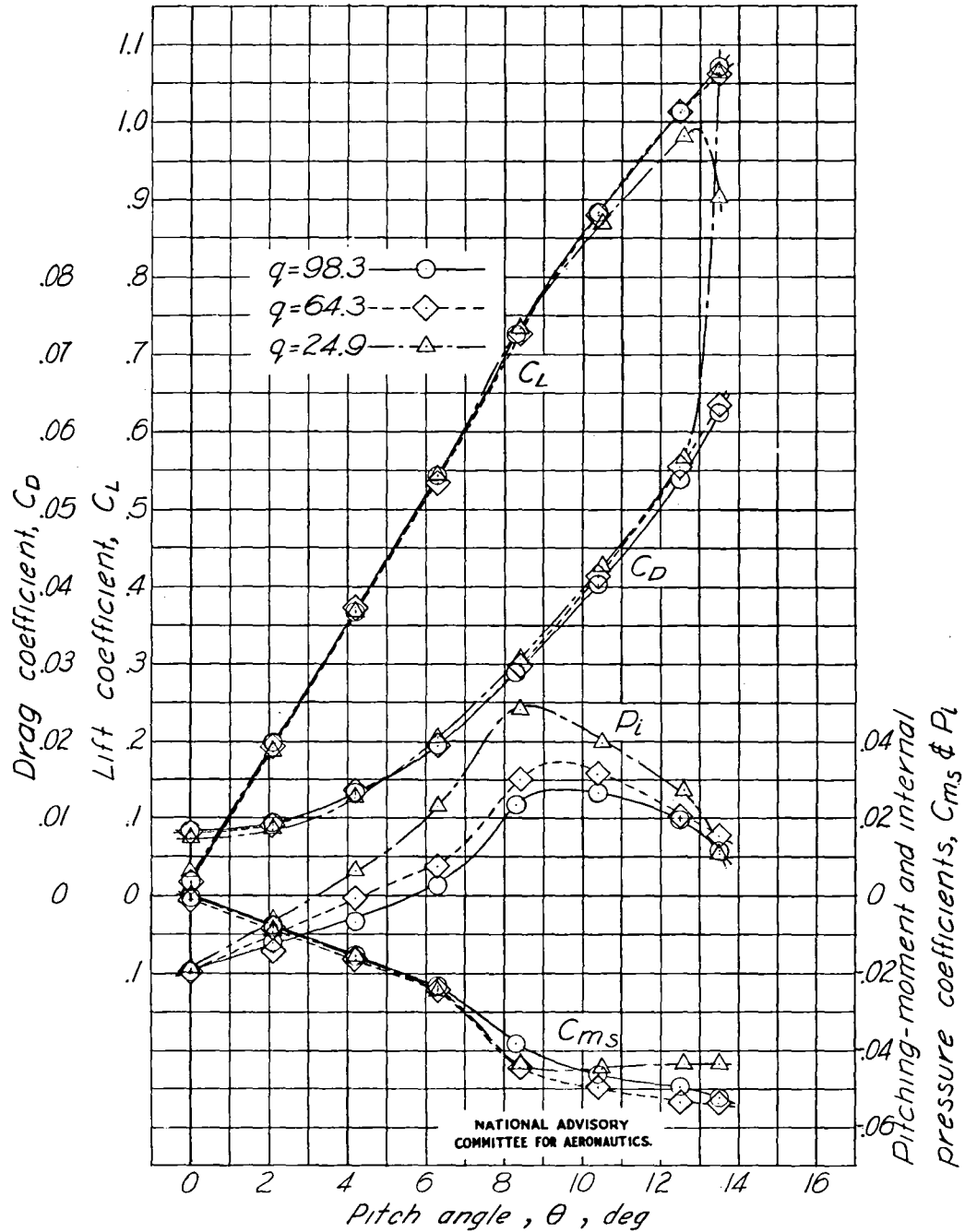


Figure 14.- Effect of dynamic pressure on the aerodynamic characteristics of the outer portion of PV-2 helicopter rotor blade, vents open.

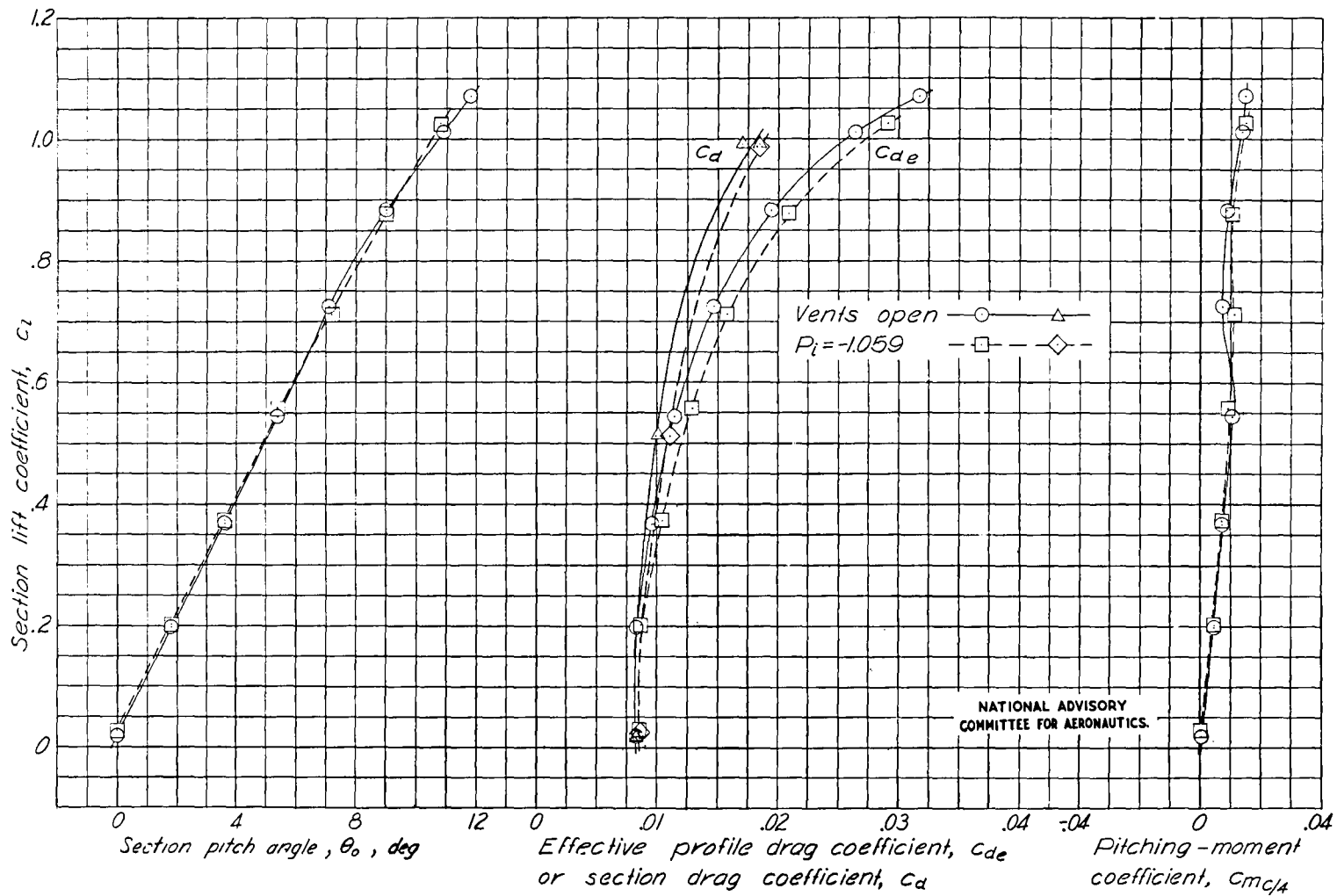


Figure 15.— Section characteristics of the outer portion of PV-2 helicopter rotor blade,  $\gamma = 0^\circ$ .

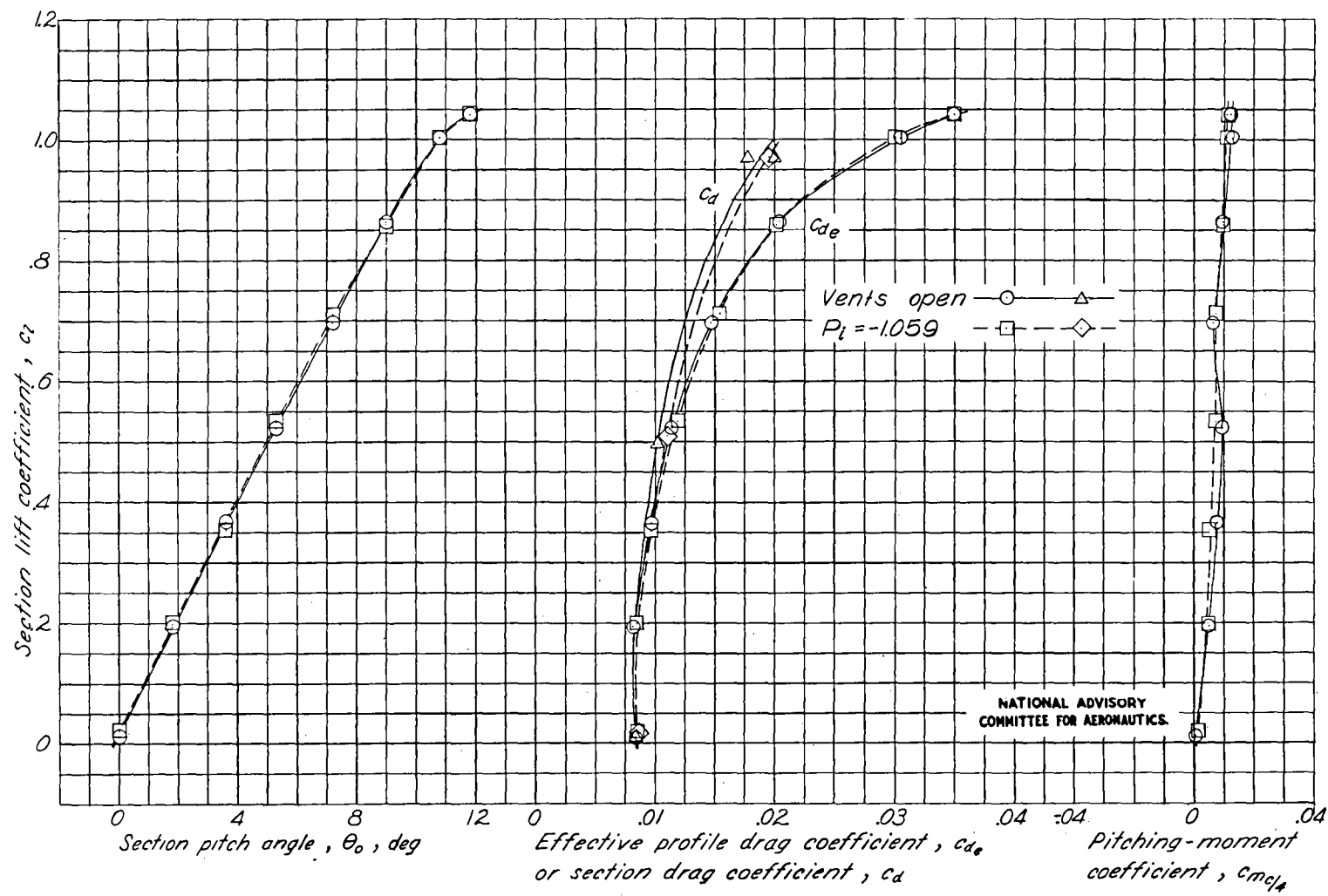


Figure 16.- Section characteristics of the outer portion of PV-2 helicopter rotor blade,  $\gamma = 5^\circ$ .

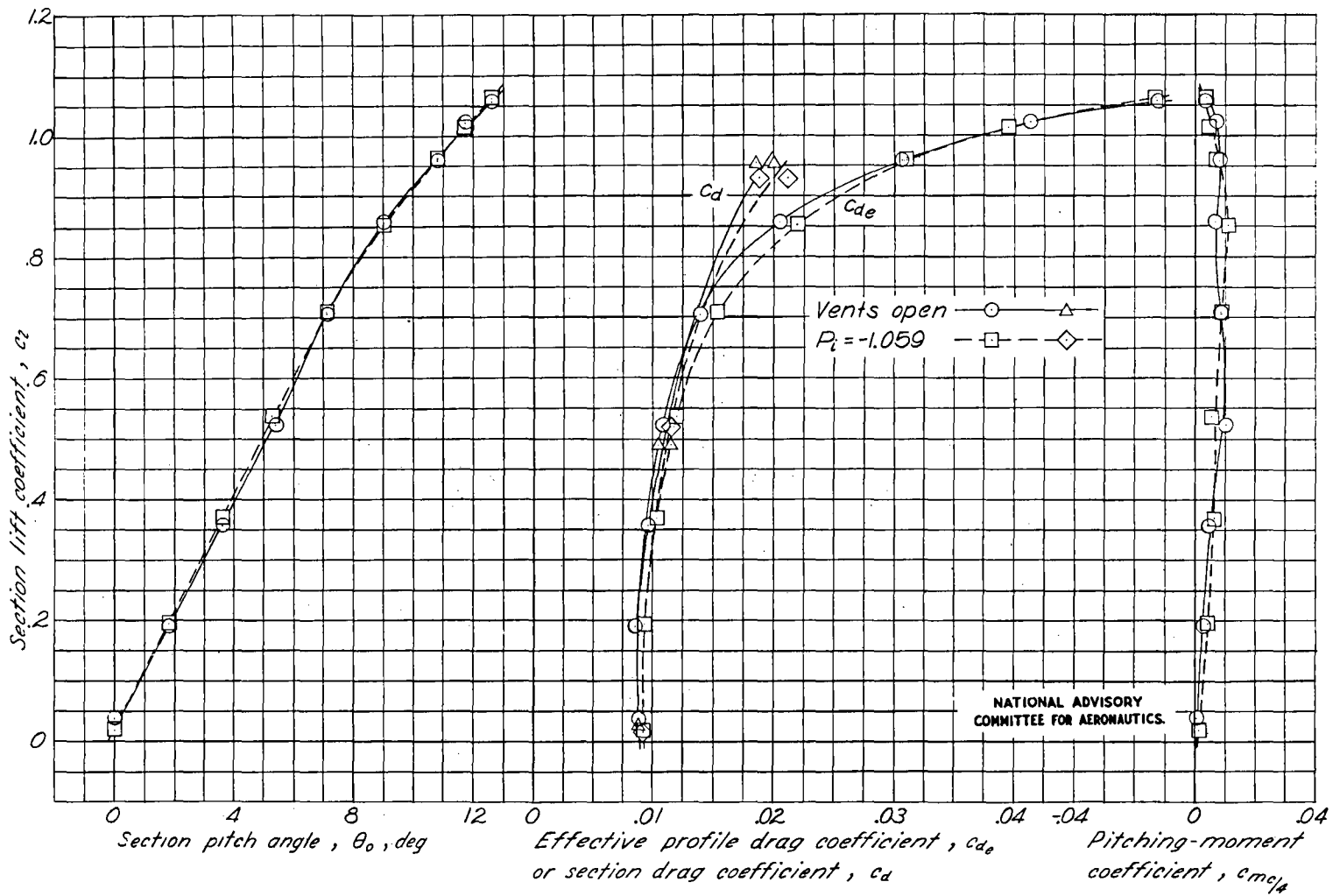


Figure 17.- Section characteristics of the outer portion of PV-2 helicopter rotor blade,  $\gamma = 10^\circ$ .

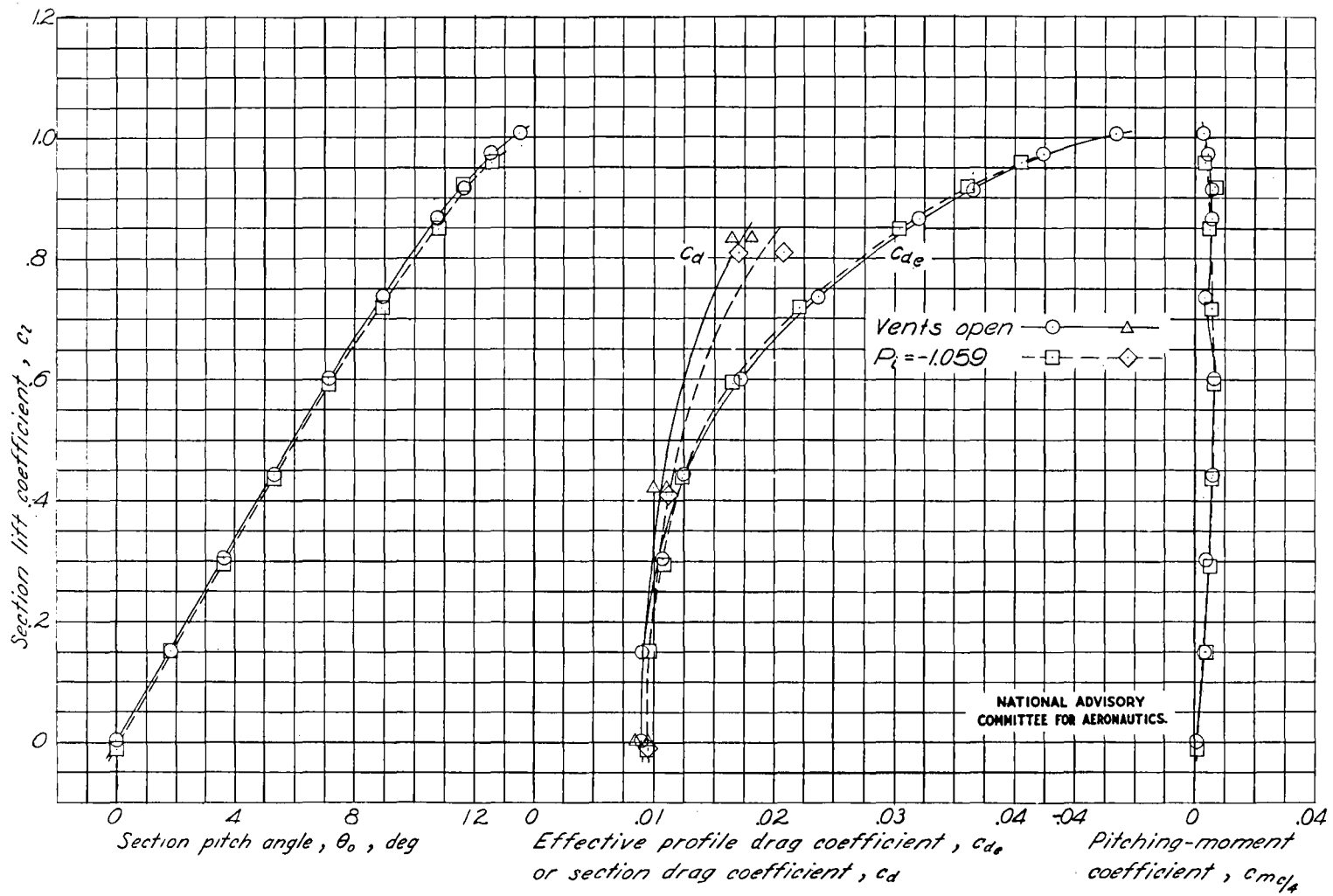


Figure 18.—Section characteristics of the outer portion of PV-2 helicopter rotor blade,  $\gamma = 20^\circ$ .

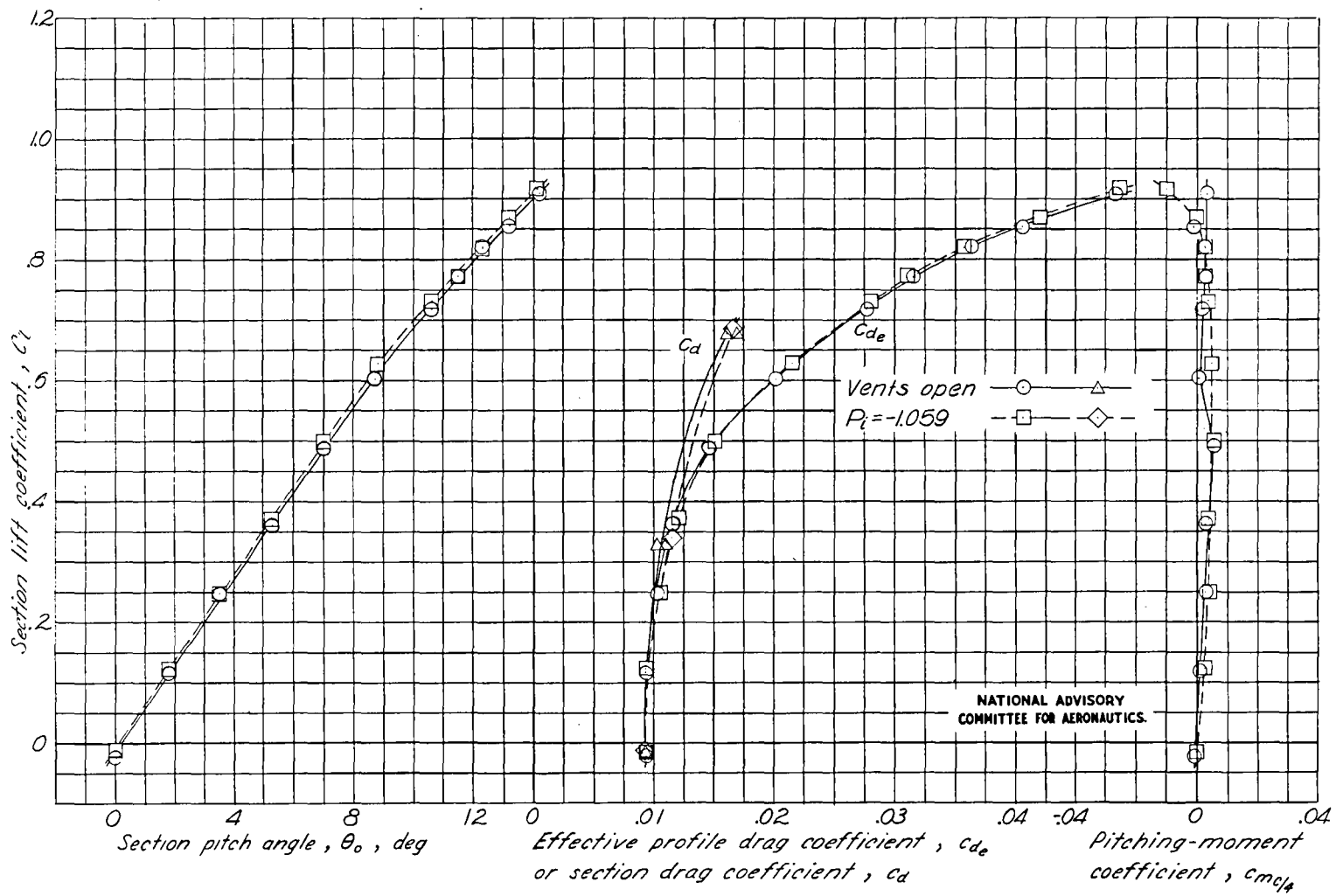


Figure 19.- Section characteristics of the outer portion of PV-2 helicopter rotor blade,  $\gamma = 30^\circ$ .

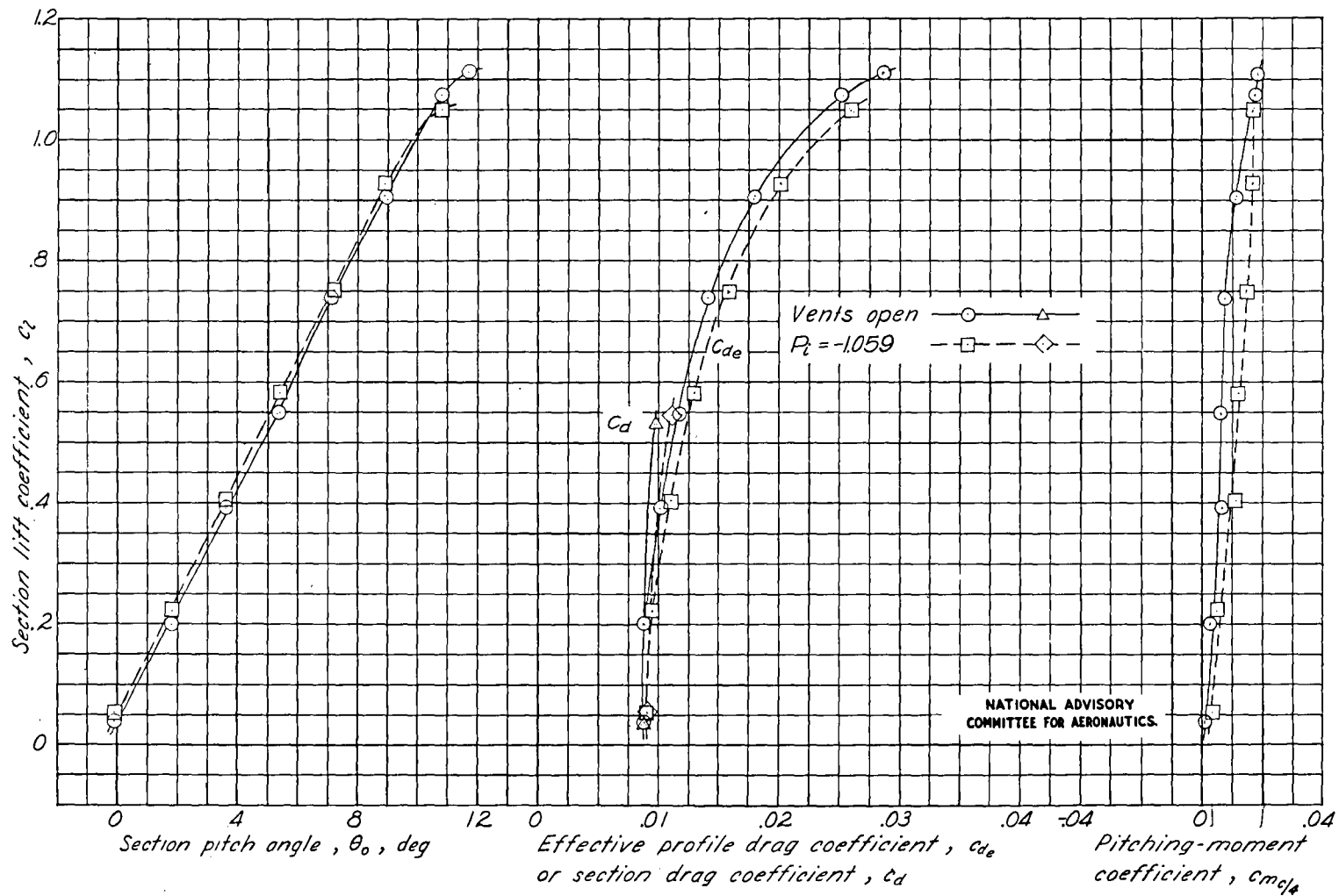


Figure 20.—Section characteristics of the outer portion of PV-2 helicopter rotor blade,  $\gamma = -5^\circ$ .

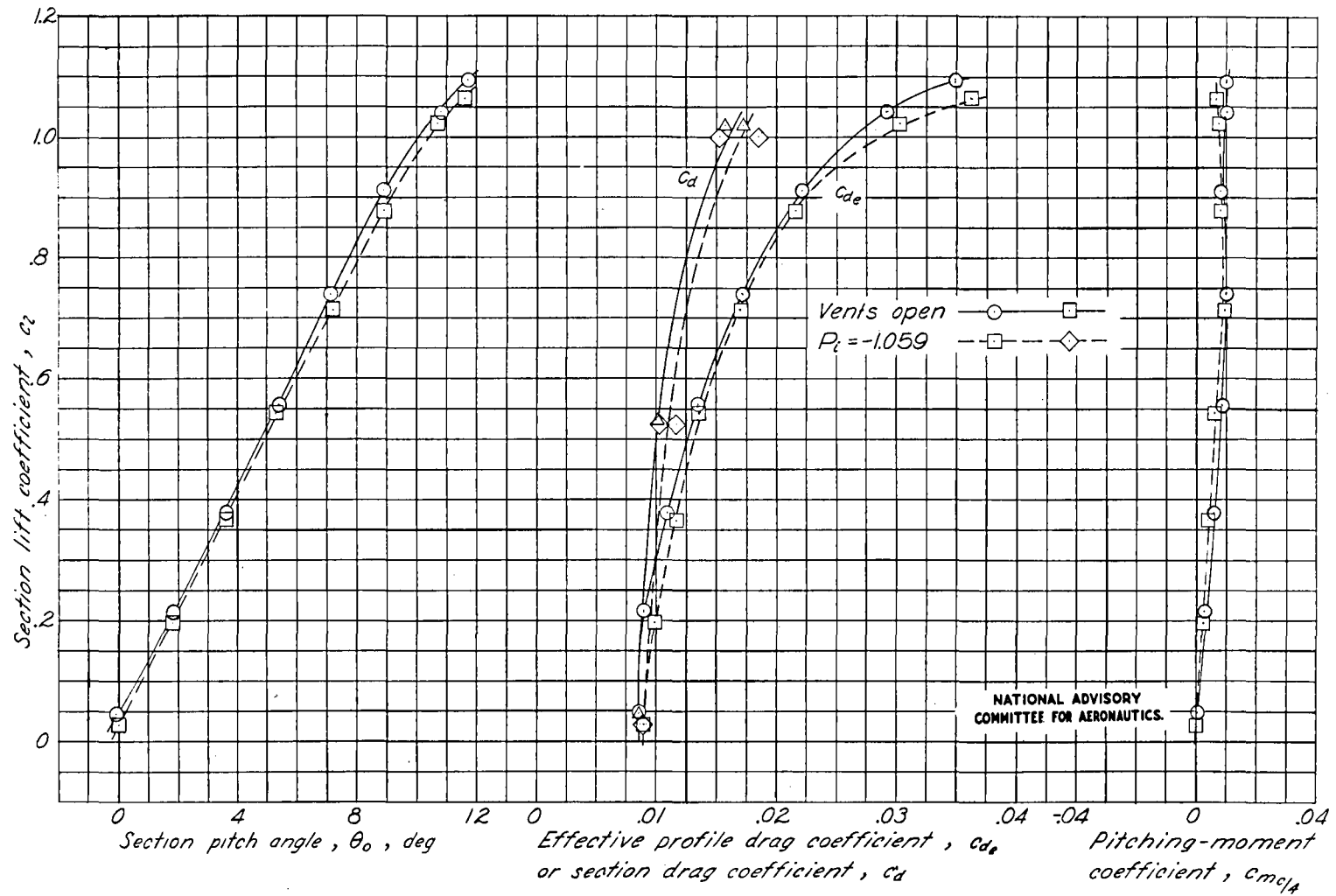


Figure 21.—Section characteristics of the outer portion of PV-2 helicopter rotor blade,  $\gamma = -10^\circ$ .

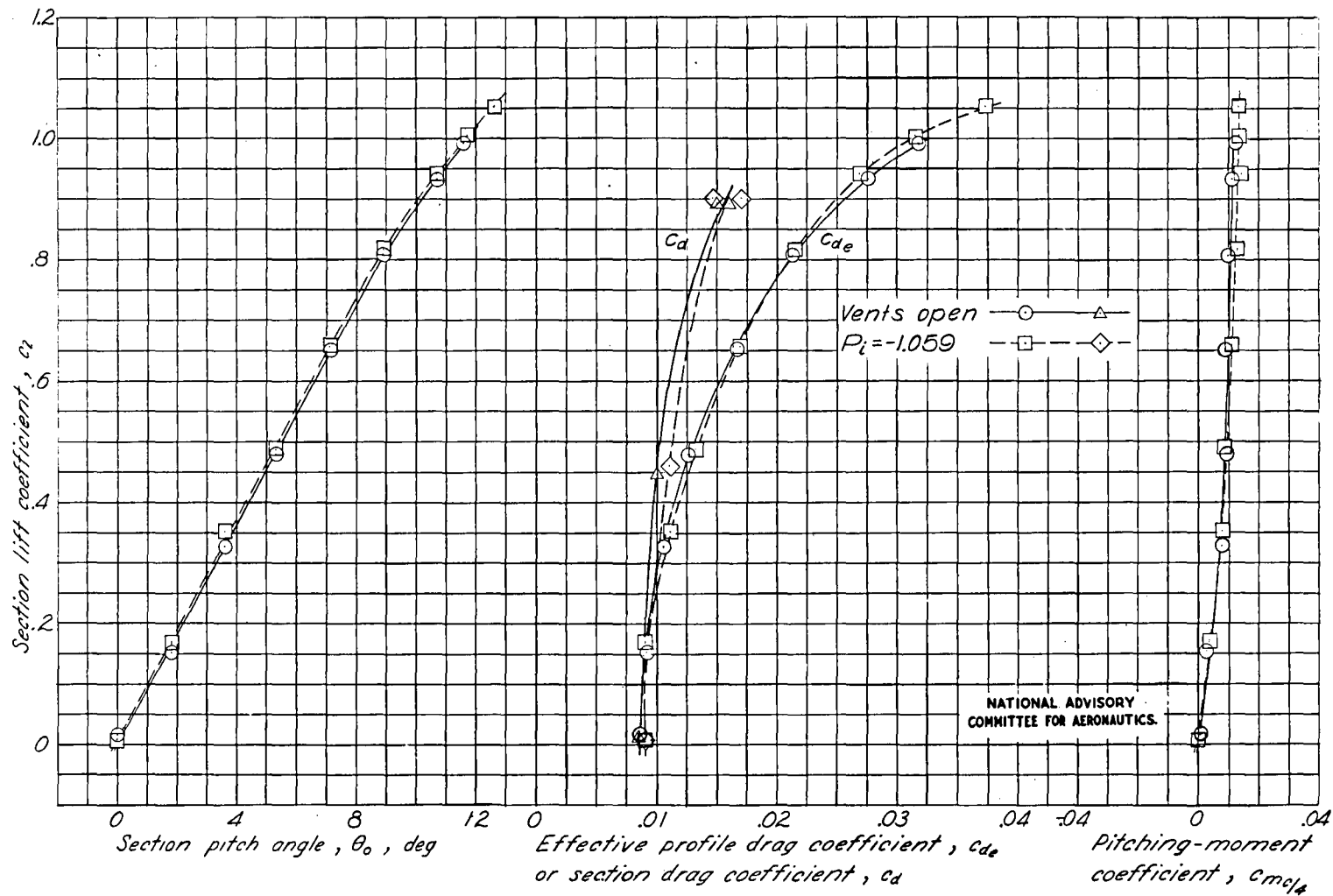
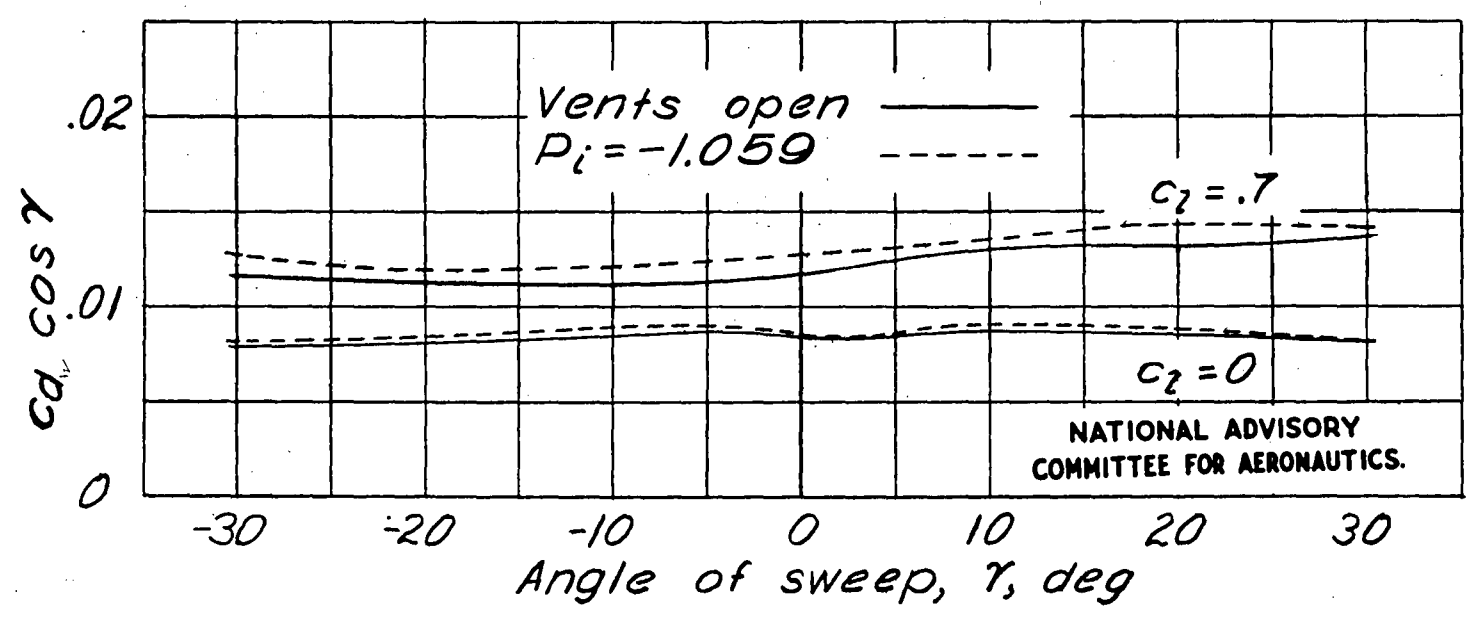


Figure 22.- Section characteristics of the outer portion of PV-2 helicopter rotor blade,  $\gamma = -20^\circ$ .





NATIONAL ADVISORY COMMITTEE FOR AERONAUTICS.

Figure 24 - Variation of  $c_d \cos \gamma$  with sweep angle.

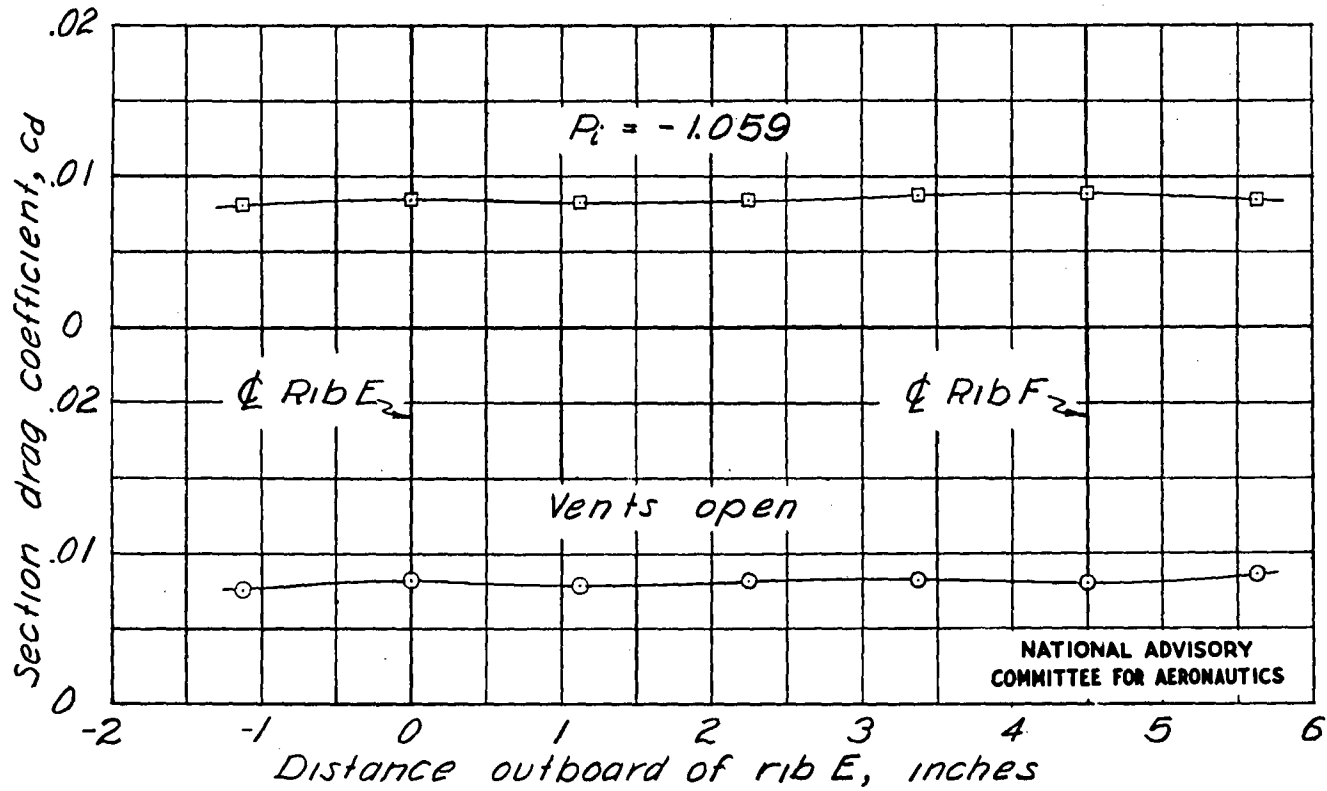


Figure 25 - Variation of section drag coefficient across panel 5 (from wake surveys),  $\gamma=0$ ,  $C_L=.015$ .

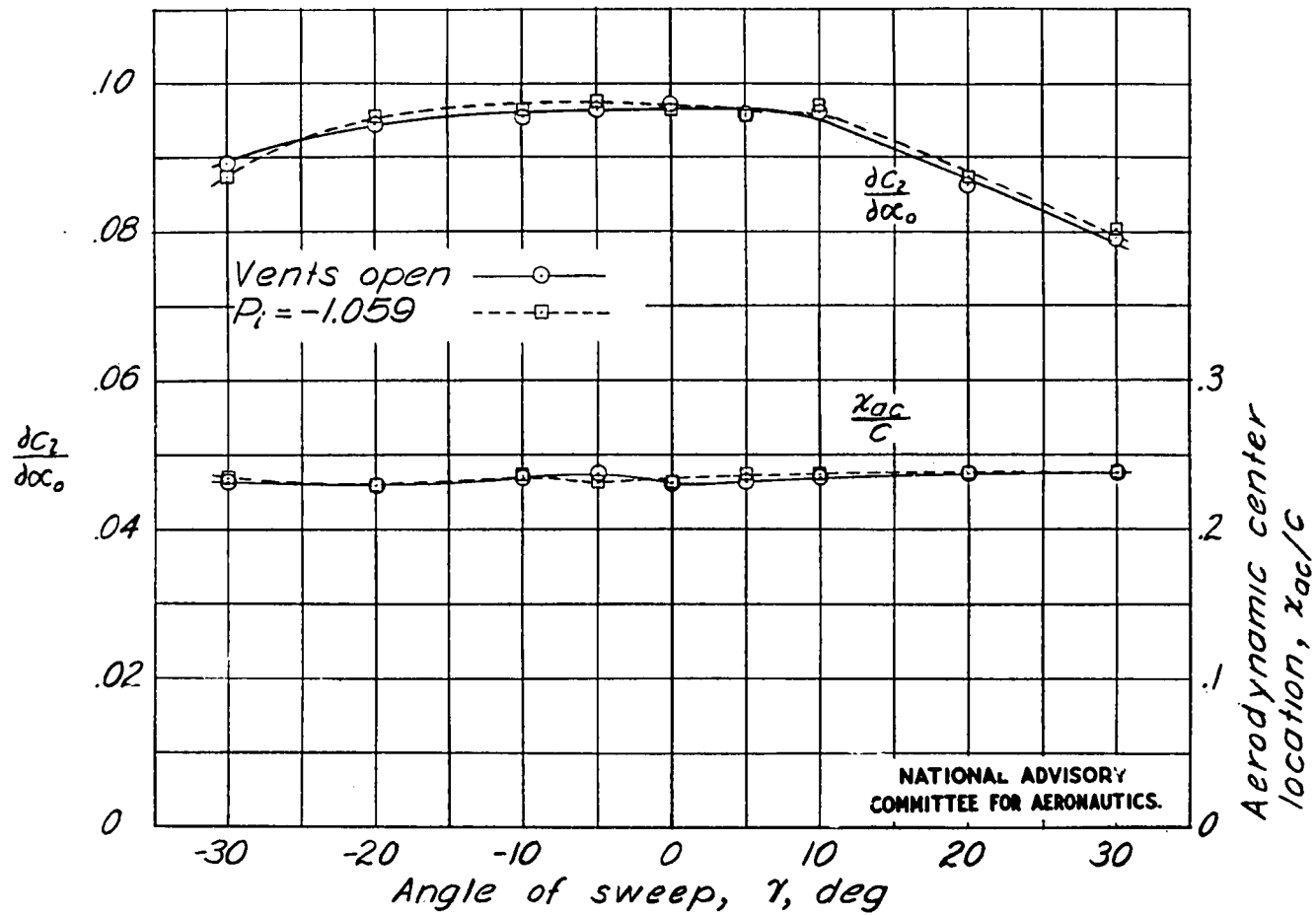
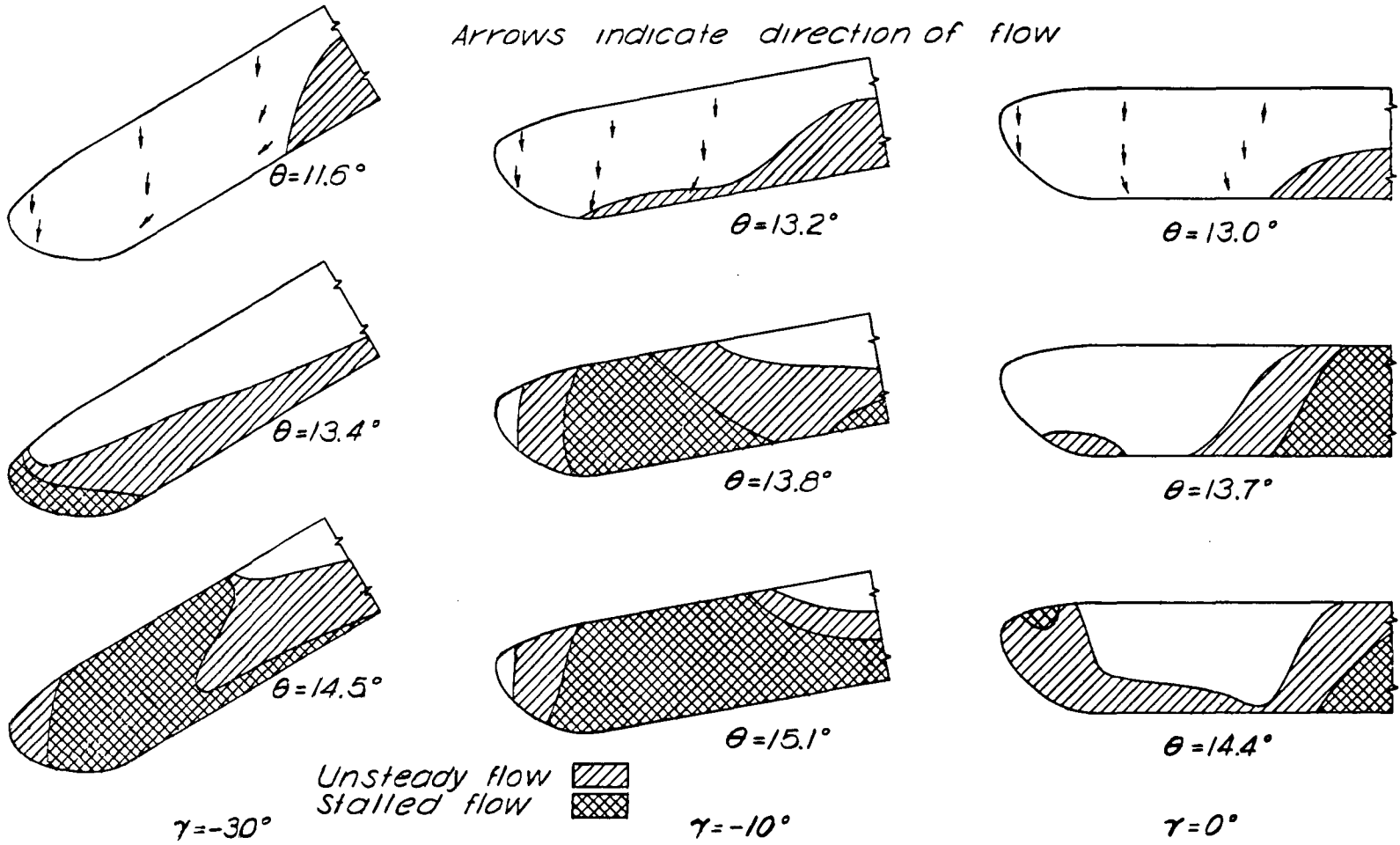


Figure 26 - Effect of sweep on  $\frac{dC_L}{d\alpha_0}$  and location of aerodynamic center.





Arrows indicate direction of flow



(b) Swept back

Figure 27 - (Concluded)

NATIONAL ADVISORY  
COMMITTEE FOR AERONAUTICS

MR No. 15C29b

**End of Document**